ELSEVIER

Nuclear Physics A 603 (1996) 117–160

NUCLEAR PHYSICS A

Quasi-elastic response functions. The Coulomb sum revisited

J. Jourdan

Departement für Physik und Astronomie, Universität Basel, CH-4056 Basel, Switzerland

Received 6 March 1996

Abstract

The world data on inclusive quasi-elastic electron scattering have been used to determine the longitudinal and the transverse response functions of ^{12}C, ^{40}Ca and ^{56}Fe. The resulting longitudinal response functions lack the "quenching" that has been one of the long-standing problems of nuclear physics.

Keywords: Electron scattering, Quasi-elastic $^{12}C(e,e')X$, $^{40}Ca(e,e')X$, $^{56}Fe(e,e')X$; Deduced longitudinal, Transverse response functions, Coulomb sum rule

1. Introduction

At momentum transfers q below 1 GeV/c and an energy loss ω of the order $\omega_{QE} \sim q^2/2M$, with M the nucleon mass, the cross section for inclusive electron scattering, (e,e'), shows a pronounced peak corresponding to scattering of the electron off a single nucleon which is ejected from the nucleus. This quasi-free peak results from an incoherent sum of elastic electron–nucleon scattering processes. The position of the quasi-elastic peak $\omega_{QE} = q^2/2M + \bar{\epsilon}$ is shifted by the average removal energy $\bar{\epsilon}$ compared to elastic scattering off the free nucleon and the width is directly related to the Fermi momentum k_F. Comparison of the early (e,e') cross section data on a series of nuclei [1] with a Fermi-gas model calculation [2] was very successful, except at large ω where Δ-excitation of the nucleon contributes. The early data of Whitney et al. [1] provided both k_F and $\bar{\epsilon}$ as a function of the nuclear mass number A.

The (e,e') cross section is a sum of the longitudinal and the transverse response function, $R_L(q,\omega)$ and $R_T(q,\omega)$, which describe the transition of the target system induced by the electron. The two response functions are related to the different ways the target can absorb the virtual photon. A separation of the two components gives

PII S0375-9474(96)00143-1

more detailed information on the target dynamics. During the last decade a number of experiments have been performed with the aim of separating the longitudinal and transverse contribution to the quasi-elastic cross section (L/T separation).

As the contribution of inelastic nucleon excitations to the longitudinal response is small, good agreement with Impulse Approximation (IA) predictions was expected for $R_L(q,\omega)$. The experimental $R_L(q,\omega)$ indeed agreed with IA calculations for nuclei with $A \leqslant 4$ over the investigated q-range 250–550 MeV/c [3–6]. However, for the nuclei ^{12}C [7], ^{40}Ca [8–10], ^{48}Ca [9,10], ^{56}Fe [9,11], and the same q-range, a common feature of the measured $R_L(q,\omega)$ was observed: The longitudinal response was significantly lower (up to 40%) than the IA prediction. This "quenching" of $R_L(q,\omega)$ was surprising and was particularly disturbing in the light of the model-independent Coulomb sum rule [12,13].

1.1. The Coulomb sum rule

Assuming for the moment *point-like* nucleons the Coulomb sum rule $C_L(q)$ is defined as the integral of $R_L(q,\omega)$ over ω,

$$C_L(q) = \int_{\omega+}^{\infty} R_L(q,\omega)\,d\omega\,, \tag{1}$$

where the energy integral is taken from $\omega+$ to exclude the elastic contribution. In a non-relativistic framework and if scattering from charged protons only is considered, $C_L(q)$ can be written in the form

$$C_L(q) = Z + Z(Z-1)f_2(q) - Z^2|F_{\mathrm{ch}}(q)|^2 \tag{2}$$

with $f_2(q)$ given by

$$f_2(q) = \frac{1}{Z(Z-1)} \int d^3r\, d^3r'\, e^{-iq(r-r')}\rho_2(r,r')\,, \tag{3}$$

where $\rho_2(r,r')$ is the two-body density, Z the atomic number of the nucleus, and $F_{\mathrm{ch}}(q)$ the elastic charge form factor. The formal derivation of the sum rule has been given in various papers [12–15].

The result for this non-energy-weighted, non-relativistic, Coulomb sum rule (CSR) is particularly elegant. $C_L(q)$ measures a property of the ground state of the nucleus and is free of complications arising from the treatment of the final state. If $\rho_2(r,r')$ is non-singular, $f_2(q)$ must fall at least as fast as some inverse power of q. Given that the nuclear elastic charge form factor falls even more rapidly with increasing q, one finds in the limit of $q \to \infty$ that $C_L(\infty) = Z$. In this limit $C_L(q)$ simply measures the number of protons in the nucleus. At finite q one expects nucleon–nucleon correlations to reduce $C_L(q)$ relative to the asymptotic limit.

The most simple correlation is due to the fermionic nature of the nucleons. Pauli correlations produce a deviation of $C_L(q)$ from Z which can be estimated using the

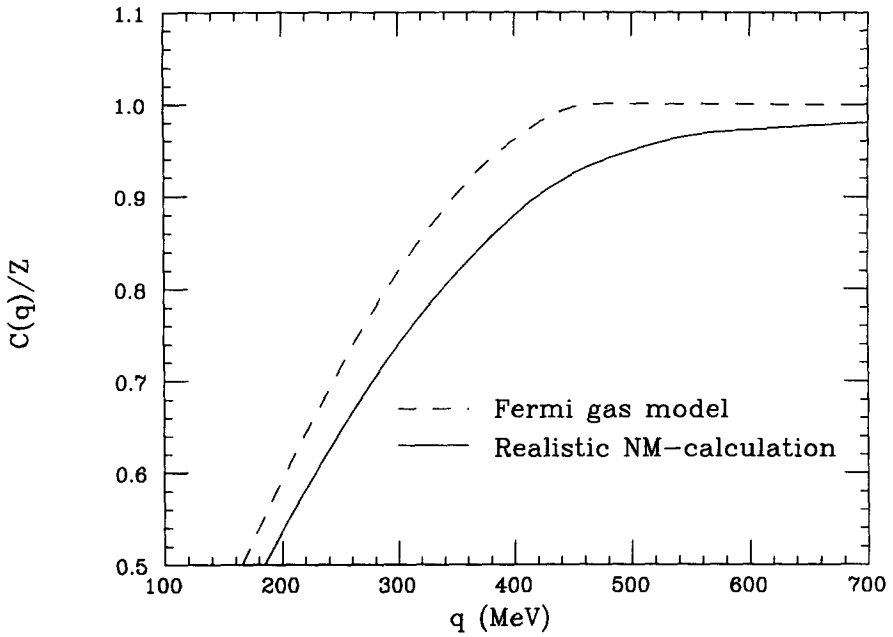

Fig. 1. CSR divided by Z for the Fermi-gas model and for the realistic nuclear matter calculation [16].

Fermi-gas model for nuclear matter. For $q > 2k_F$ these correlations vanish since the Pauli exclusion principle is satisfied for all nucleon momenta. For these q-values deviations of the CSR from the value Z measure short-range correlations between nucleons in the nuclear system. Fabrocini and Fantoni [16] studied $C_L(q)$ as a function of q within the framework of a non-relativistic nuclear matter calculation, treating 1p1h and 2p2h excitations for both initial and final states exactly. They found that, due to short-range correlations, the approach to saturation is much slower than suggested by the (uncorrelated) Fermi-gas model. This additional reduction is clearly displayed in Fig. 1 where the CSR is shown as a function of q for the Fermi-gas model and for the realistic nuclear matter calculation.

To determine short-range nucleon–nucleon correlations through a measurement of the deviation of the CSR from the asymptotic value was the original motivation of an experimental determination of the CSR. Already McVoy [13] predicted the effect of such correlations to be of the order of 5–10% for $q \sim 500$–$600\ \mathrm{MeV}/c$. The experimental results, however, suggested a suppression of up to 40% at $q = 550\ \mathrm{MeV}/c$ for medium A-nuclei, a result that was incompatible with all predictions including the most recent nuclear matter calculations.

As the Coulomb sum rule does not depend on the nuclear model, the "missing strength" was not easily understood, and motivated a large theoretical effort. A rather complete review of this theoretical work in connection with the sum rule is given by Orlandini and Traini [15]. With increased sophistication of the calculations, the original discrepancy has been reduced somewhat, but no calculation has been able to reproduce the longitudinal response function without damaging the agreement with the transverse

one.

The assumption of point-like nucleons made above is of course not satisfied in reality. In an experimental determination of the CSR the nucleon charge form factor, which accounts for the finite nucleon size, has to be divided out before $R_L(q,\omega)$ is used in Eq. (1). This additional factor in $C_L(q)$ could also provide an explanation for the difficulties encountered in understanding the experimental strength. Indeed, the most popular interpretation assumed that the charge radius (but not the magnetic radius) of the nucleon increases in the nuclear medium, as a consequence of a partial deconfinement of the quarks inside the nucleon (swollen nucleons) [17–20]. An increase in size decreases the nucleon charge form factor, thus leading to a reduced $R_L(q,\omega)$. Modifications of the nucleon radius by up to 30% have been proposed.

However, restrictive limits on a possible radius change resulted from a study of the scaling function $F(y)$ extracted from inclusive quasi-elastic cross section data on ^{3}He and ^{56}Fe taken over a large range of q [21,22]. The y-scaling property in inclusive (e,e') scattering is very sensitive to a change of the nucleon radius, as this would lead to a change of the elementary electron–nucleon cross section which is divided out before scaling is observed. The experimental result limited a possible radius change to 2%, with an error bar of (+1%,-4%). In the kinematical regime of the data used, the longitudinal contribution was about $\sim$ 30%, which results in a limit on the change of the *charge* radius of about 6%. This is far too low to explain the observed suppression of $R_L(q,\omega)$ at high q.

1.2. New determination of the CSR

Despite the large efforts spent on measuring data suitable for L/T separations, one can not help to note that the consistency of the experimental data is less than satisfactory. New measurements on ^{40}Ca [23], together with the data of Deady et al. [10], yield a longitudinal response function which differs markedly ($\sim$ 30%) from previous determinations in the q-range from 300 MeV/c to 450 MeV/c. Measurements on ^{208}Pb [24] show a reduction of $\sim$ 50% of the Coulomb sum at q = 550 MeV/c whereas no quenching is observed for ^{238}U [25]. This is not understood as quasi-elastic scattering is expected to measure bulk properties which do not depend on the specific nucleus considered.

One also can not help to note that the "quenched" longitudinal response functions show a somewhat unphysical behaviour at large ω and q. When determining $R_L(q,\omega)$ over the full range of ω accessible with the published data, negative (unphysical) response functions are found at an energy loss beyond the one shown in the various publications (Fig. 2).

In this paper I will demonstrate that the quenching to a large degree results from the limited significance of the data used. All previous separations only considered data from a *single* experiment, performed with electron accelerators of energies in the $\leqslant$ 700 MeV range. At these energies cross sections at the higher q-values, which are of main interest for the CSR, could not be measured at very forward scattering angles. As a consequence,

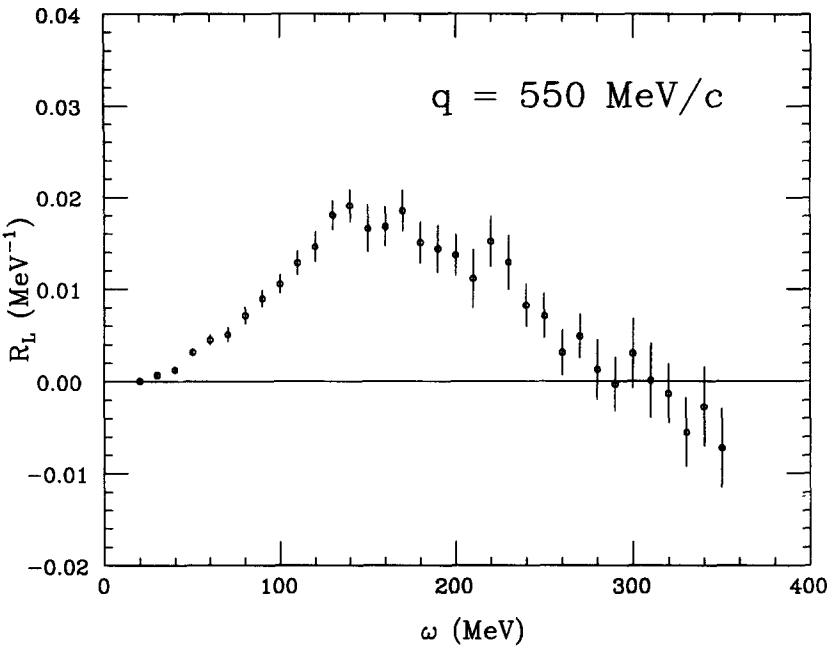

Fig. 2. $R_L(q,\omega)$ for ^{40}Ca obtained using the published cross section data of [9].

the data covered only about 1/2 of the possible range of the virtual photon polarization ϵ. This precluded a maximization of the contribution of $R_L(q,\omega)$ to the total response and made the determination sensitive to systematic errors. To improve the determination of $R_L(q,\omega)$ a larger ϵ-range has to be employed for the separation, by including data at higher energy and much more forward angle.

All available world data on inclusive quasi-elastic scattering from ^{12}C, ^{40}Ca, and ^{56}Fe are used in the present study. The experiments which provide the high-energy/forward-angle data most relevant in an L/T separation of the world data have been described in Refs. [26,27]. More detailed accounts are given in various thesis works [28,29]. The combined world data cover almost the full ϵ-range ($0 \leqslant \epsilon \leqslant 1$) with typical values from 0.05 to 0.95 for all nuclei considered.

Besides the use of the world data, a detailed study of the validity of the plane-wave Born approximation (PWBA) for the L/T separation is performed in the present work. Corrections for Coulomb distortion, neglected in the past for the nuclei in question, are included in the present analysis and found to be important. The results on the response functions are compared to the most recent theoretical calculation that describes consistently correlations and the nucleon–nucleus interaction in both the initial and final states [16].

The values of $R_L(q,\omega)$ extracted are used to determine an experimental value of the Coulomb sum. In the determination of the CSR a careful analysis of the corrections to be applied is performed. The CSR, as defined in Eq. (1), is only valid for point-like protons and in a non-relativistic framework. These assumptions are not strictly

valid, and appropriate corrections to the experimental results have to be applied before a comparison with theory can be discussed. The role of the nucleon form factor and relativistic corrections are studied in detail. One should note that a consistent treatment of all the corrections has not been applied when extracting the CSR in the past.

The layout of the paper is as follows: In the next section the formalism used for the determination of the response functions is reviewed, followed by a discussion of the corrections for Coulomb distortion. Section 3 discusses the available world data emphasizing considerations on the role of systematic errors. In Section 4 and 5, results on the response functions for ^{12}C, ^{56}Fe, and ^{40}Ca are presented and compared to theoretical calculations. The results are used in Section 6 to determine the Coulomb sum. The conclusions are given in Section 7.

2. Extraction of response functions

2.1. Formalism

The plane-wave Born approximation (PWBA) cross section for inclusive inelastic (e,e') scattering can be written as [30]

$$\frac{d^2\sigma}{d\Omega\, dE'} = \sigma_{\mathrm{Mott}} \left(\left(\frac{Q}{q}\right)^4 R_L(q,\omega) + \left(\frac{Q^2}{2q^2} + \tan^2\vartheta/2\right) R_T(q,\omega) \right), \tag{4}$$

where ϑ is the scattering angle of the electron and $Q^2 = q^2 - \omega^2$ the four momentum squared of the virtual photon. The Mott cross section is defined as

$$\sigma_{\mathrm{Mott}} = \left(\frac{\alpha \cos\vartheta/2}{2E \sin^2\vartheta/2} \right)^2, \tag{5}$$

with E the incident energy of the electron and α the fine structure constant.

The procedure used in this work to separate $R_L(q,\omega)$ and $R_T(q,\omega)$ is as follows. The quantity

$$\Sigma(q,\omega,\epsilon) = \frac{d^2\sigma}{d\Omega\, dE'} \frac{1}{\sigma_{\mathrm{Mott}}} \epsilon \left(\frac{q}{Q}\right)^4 = \epsilon R_L(q,\omega) + \frac{1}{2}\left(\frac{q}{Q}\right)^2 R_T(q,\omega) \tag{6}$$

is plotted as a function of the virtual photon polarization ϵ which is defined as

$$\epsilon = \left(1 + \frac{2q^2}{Q^2} \tan^2\vartheta/2\right)^{-1} \tag{7}$$

and varies from 0 to 1 as the scattering angle ϑ ranges from 180 to 0 degrees. In this approach $R_L(q,\omega)$ is the slope, and $\frac{1}{2}(q/Q)^2 R_T(q,\omega)$ is the intercept of a linear fit to the data. Data measured at 180 degrees can easily be included in a separation within this approach.

2.2. Coulomb corrections

Eq. (6), which is used to separate the response functions, is only valid in the PWBA and it only can be applied to data after the cross sections are corrected for Coulomb distortion of the electron wave functions. Such Coulomb distortion effects have been neglected in the analyses of [7–11], but are included in the present one.

The distorted-wave functions of the electron are obtained by solving the Dirac equation for an electron in the spherically symmetric static Coulomb potential $V_c(r)$ of the nuclear charge distribution. This can be done without approximation by making a partial-wave expansion of the electron waves and solving the resulting radial equations numerically. In the past numerical solutions have routinely been obtained for elastic and inelastic scattering to discrete states [31]. More recently, Jin et al. [32,33] have used such a complete distorted-wave Born approximation (DWBA) approach to calculate quasi-elastic $(e,e'p)$ and (e,e') scattering. For inclusive quasi-elastic (e,e') scattering the exact treatment of Coulomb distortion still requires a large computational effort.

Various approximate treatments have been proposed in the past to account for Coulomb distortion. Lenz and Rosenfelder [34] introduced a "high-energy expansion" for the scattering states in which the radial part of the wave function is written in terms of spherical Bessel functions with a modified argument. The coefficients are expanded in inverse powers of the electron wave number k, taking into account terms up to second order. Furthermore, the scattering phases can be approximated as a constant plus a $j(j+1)$ term which can be replaced by the operator $\boldsymbol{J}^2$, where $\boldsymbol{J} = (\boldsymbol{L}+\frac{1}{2}\sigma)$ is the total angular momentum operator and σ the spin operator which acts on the Pauli spinors u_h. As a result one gets an analytic solution for the incident $(+)$ and the scattered $(-)$ electron wave function of the form

$$\Phi_h^{\pm} = e^{i\delta_{1/2}}\eta(r)e^{\pm ib(\boldsymbol{J}^2-3/4)}e^{ikr\eta(r)}u_h \tag{8}$$

with

$$b = -\frac{1}{2k^2}\int_0^{\infty}\frac{1}{r}\frac{dV_c}{dr}dr\,, \tag{9}$$

$$\delta_{1/2} = -Z\alpha\ln(2kR) - \int_0^{R} V_c\,dr + b\,. \tag{10}$$

The radial function

$$\eta(r) = \frac{1}{kr}\int_0^{r}(k - V_c(r'))dr' \tag{11}$$

takes into account the change in amplitude and wave number due to the Coulomb potential. Lenz and Rosenfelder [34] showed that such an approximation is valid provided $j + 1/2 \ll kR$, where R is the radius within which the entire charge distribution lies.

The effect of the Coulomb potential can be qualitatively explained in the following way. First, the potential leads to an acceleration (deceleration) of the incident (scattered) electron. At the moment of interaction the electron then has an increased wave number $k_{\text{eff}} = k\eta(r)$. Second, due to the attractive force, the electron wave has an increased amplitude in the vicinity of the nucleus, an effect which often is referred to as "focusing effect".

If the $e^{\pm ib(J^2-3/4)}$ term of Eq. (8) is expanded to zeroth order in αZ one obtains the well-known "effective momentum approximation" (EMA) [35]. In this approximation the electron waves are plane waves with the effective wave number $k_{\text{eff}} = k\eta(r) = k - V_c(0)$, where $V_c(0)$ is the Coulomb potential at the origin. The "focusing effect in leading order" is accounted for by multiplying the cross section with the renormalization factor $(k_{\text{eff}}/k)^2$. It should be noted, however, that when replacing q with q_{eff} this focusing effect is cancelled by the $1/E^2$ term of the Mott cross section [36].

An extension of the EMA has first been used by Knoll [37] to describe transition form factors for low-lying states of ^{208}Pb. For high momentum transfers and when retaining terms to first order in αZ, Knoll obtained quantitative agreement with the exact DWBA calculation. A generalization to quasi-elastic (e, e') scattering has been proposed by Traini et al. [38]. It has been suggested that retaining second-order terms in αZ in the phase shifts [38] leads to a focusing term which, however, is small for the kinematics and targets studied in this work [39]. From the work of Traini et al. [39] one tends to conclude that it is safe to use EMA to correct for Coulomb distortion.

Two observations spoil the validity of this simple treatment: The overall correction of the second-order expansion of Traini et al. [38] is negative and consequently *decreases* the focusing of the electron wave, indicating that the αZ expansion has not converged. A similar observation can be made in Fig. 2 of Ref. [38] where the longitudinal cross section for $(e, e'p)$ from the $3s$ state in ^{208}Pb is calculated in zeroth, first, and second order in αZ. The difference between the zeroth- and the first-order cross section is as large as the difference between the first and the second-order cross section.

If one compares the (e, e') cross section for ^{56}Fe calculated in the EMA with the result of an "exact" DWBA calculation [40] for kinematics typical for the present work (Fig. 3), one observes that EMA fails to reproduce the exact result. According to the comments made above, the second-order expansion of Traini [39] can not improve upon this discrepancy.

It has been observed by Wright [41] that the dominant contribution to the quasi-elastic cross section is due to impact parameters of the order of the nuclear radius R. This leads to large j-values for which an expansion of the $e^{\pm ib(J^2-3/4)}$ term is questionable and the approximation $j + 1/2 \ll kR$ is no longer accurate. Wright proposes an alternative approximation in which this observation is accounted for.

Two modifications are proposed. First, in order to take into account the correct phase variation for high j-values, the phase dependence in Eq. (8) is extended to

$$\delta_j = \delta_{1/2} + (J^2 - 3/4)\beta_1 + (J^2 - 3/4)^2\beta_2 , \tag{12}$$

where β_1 and β_2 are parameters fitted to the solution of the exact DWBA calculation.

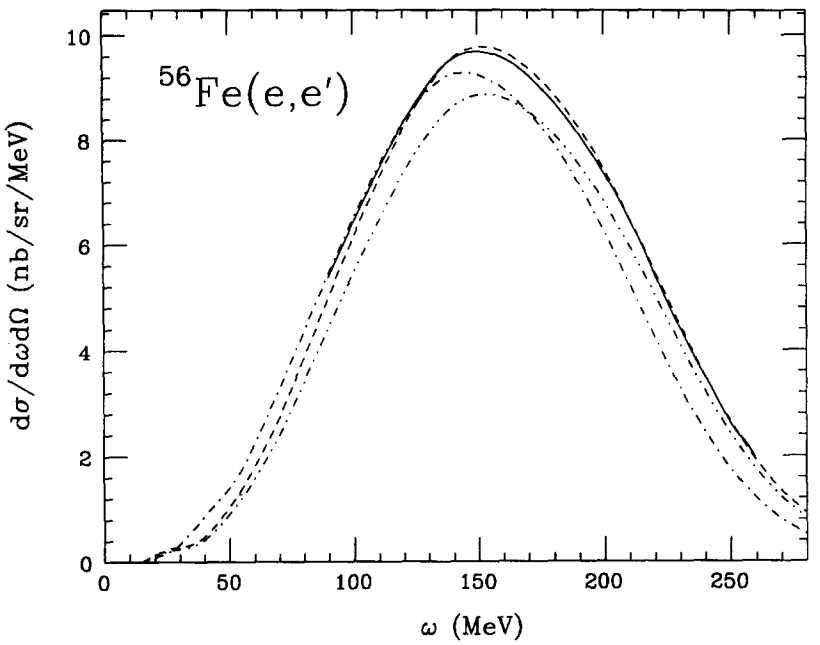

Fig. 3. Comparison of the different approximations used to include Coulomb effects in the calculation of the inclusive quasi-elastic cross section ^{56}Fe(e,e') at $E = 400$ MeV, $\vartheta = 90°$. The exact DWBA result (solid), the PWBA result (dot-dash), the result in EMA (dot-dot-dash), and LEMA (dash) are shown.

This extension is particularly important for the high j-values relevant in the description of exclusive quasi-elastic $(e,e'p)$ which is sensitive to a proper description of the phase variation. Inclusive (e,e') scattering is much less sensitive to details of the phase, however, and it is found that neglecting the phase variation (i.e. $\beta_1 = \beta_2 = 0$) still results in a more accurate description than expanding the exponential factor with a large argument.

A second consequence of the large impact parameters is the fact that the electron does not feel the Coulomb potential at the origin, $V_c(0)$, but rather the potential near the surface of the nucleus. Lenz and Rosenfelder showed that the argument of the spherical Bessel functions in the approximate radial solutions are functions of $k_{\text{eff}}r$, where the incident and scattered wave number of the electron is given by

$$k_{\text{eff}} = k - \frac{1}{r}\int_0^r V_c(r')dr' . \tag{13}$$

In this expression the integral corresponds to the Coulomb potential $V_c(r)$ near the surface of the nucleus. As this effective momentum enters the effective momentum transfer in the Fourier transform, the resulting response function is a very sensitive function of the choice of k_{eff}. Wright has shown that replacing $V_c(r)$ by $V_c(0)$ is not a good approximation. In fact, taking the effective wave number into account properly is much more important than including the scattering phase shifts when analyzing inclusive (e,e') scattering.

The approximate treatment of the Coulomb distortion in quasi-elastic (e, e') scattering including these modifications will in the following be called "local effective momentum approximation" (LEMA). LEMA is in much better agreement with the exact DWBA calculation as is demonstrated in Fig. 3. The approximation will be described in more detail by Wright et al. [41].

In the following I discuss how the data have been corrected for Coulomb distortion using the results of Wright et al. [40]. In order to study the improvements arising from the exact treatment the data in a first step are corrected as is done in EMA, with $V_c(0)$ in k_{eff}. The incident and scattered energies of the electrons are replaced by the effective values given by

$$E_{\text{eff}} = E - V_c(0)\,, \tag{14}$$

$$E'_{\text{eff}} = E' - V_c(0)\,, \tag{15}$$

using $V_c(0) = -\frac{3}{2}Ze^2/R$ with R the nuclear radius. Then the experimental cross sections are renormalized to account for the leading-order "focusing" effect via

$$\frac{d^2\sigma_{\text{EMA}}}{d\Omega\, d\omega} = \frac{d^2\sigma_{\text{exp}}}{d\Omega\, d\omega}\left(\frac{E}{E_{\text{eff}}}\right)^2 . \tag{16}$$

Note that such a correction *reduces* the experimental cross section values. These corrected cross sections including the corrected kinematics have then been used to interpolate and extract total response functions $\Sigma^{\text{EMA}}(q, \omega, \epsilon)$ for a given q-value. If the EMA would correctly account for Coulomb distortion these response functions would already be PWBA response functions to be used in an L/T separation.

However, knowing that the LEMA gives a better parameterization of the exact Coulomb distortion one needs to use, in a second step, the following relation to extract PWBA response functions:

$$\Sigma_{\text{PWBA}}(q, \omega, \epsilon) = f(q, \omega, \epsilon)\, \Sigma_{\text{EMA}}(q, \omega, \epsilon)\,. \tag{17}$$

The correction factor $f(q, \omega, \epsilon)$ is the ratio of a PWBA model response function divided by a model response function calculated in LEMA and corrected for Coulomb distortion in the EMA approach as described for the data above. The model used to calculate the cross sections is described in Section 4 and Ref. [32].

We find that the correction factors for the longitudinal (f_L) and the transverse (f_T) contribution are different, particularly at large ω. Thus, Eq. (17) in principle can not be used directly to determine PWBA response functions (which are a mixture of longitudinal and transverse contributions). An iterative procedure has to be used. One starts the iterative procedure with

$$\Sigma_{\text{PWBA}_1}(q, \omega, \epsilon) = f_T w_1(\omega, \epsilon)\, \Sigma_{\text{EMA}}(q, \omega, \epsilon) \tag{18}$$

with $w_1(\omega, \epsilon) = 1$ for the first iteration. This takes care of the dominant correction as $f \sim f_T$ because Coulomb distortion is largest in kinematic regions which are dominated by the transverse response. With the separated response functions of the $(n-1)$th

iteration one can calculate the weighting factors $w_n(\omega, \epsilon)$ which take care of the longitudinal contribution. Convergence of this procedure is very fast as the correction term to $w_1(\omega, \epsilon) = 1$ gives a very small contribution, either because $f_T - f_L$ is negligible or because ϵ and $R_L(q, \omega)$ are small. In fact an L/T separation using just Eq. (17), avoiding the iterative procedure, gives results which agree within 0.5% with the fully iterated result.

The procedure has been checked treating the LEMA-calculated cross section values as experimental data. Once these model cross sections are corrected for Coulomb distortion the separated $R_L(q, \omega)$ and $R_T(q, \omega)$ values are indistinguishable from the results of the PWBA input.

In order to see the effect of the Coulomb distortion on the individual response functions $R_L(q, \omega)$ and $R_T(q, \omega)$, cross sections have been calculated in PWBA and in LEMA followed by an L/T separation in which Coulomb distortion is ignored. The results are shown in Fig. 4 for ^{56}Fe at $q = 570$ MeV/c. For $R_L(q, \omega)$ the effect of ignoring the Coulomb distortion (dashed) is a shift of the response towards smaller ω and a decrease of the peak value. At large ω it can lead to negative $R_L(q, \omega)$ values. The results for the two lower q-values are qualitatively similar. The largest decrease of the peak value of $R_L(q, \omega)$ is observed for ^{56}Fe at $q = 300$ MeV/c where it amounts to 6%.

3. Data

In the following I discuss the data used in the present L/T separation. As the various experiments on quasi-elastic (e, e') data did not coordinate the kinematics for a global L/T separation, the kinematical overlap is not ideal and restricts the choice of possible q-values. In the present work the q-values chosen are 300 MeV/c, 380 MeV/c and 570 MeV/c.

3.1. Kinematics

In Fig. 5 the kinematical locus of the high-energy/forward-angle data from the SLAC experiments is shown as a function of q and ω. The two spectra from Day et al. [26] (NE3) were measured for an incident energy of 2.0 GeV and scattering angles of 15 and 20 degrees. These data, which have been measured on ^{12}C, ^{27}Al, ^{56}Fe, and ^{197}Au, are most valuable for the L/T separation at high q. The choice of $q = 570$ MeV/c minimizes the corrections for these data due to the interpolation, in particular at high ω as will be discussed in Section 4.

Six spectra were measured in the experiment of Baran et al. [27] (NE1) over a large range of ω for incident energies of 1.3, 1.5 and 1.65 GeV and scattering angles of 11.9 and 13.5 degrees. Data of this experiment have been measured on ^{12}C and ^{56}Fe. The boundaries of the q–ω region covered by these data are also indicated in Fig. 5. The q-values of 300 and 380 MeV/c have been selected to maximize the q-range of the response functions extracted from the world data.

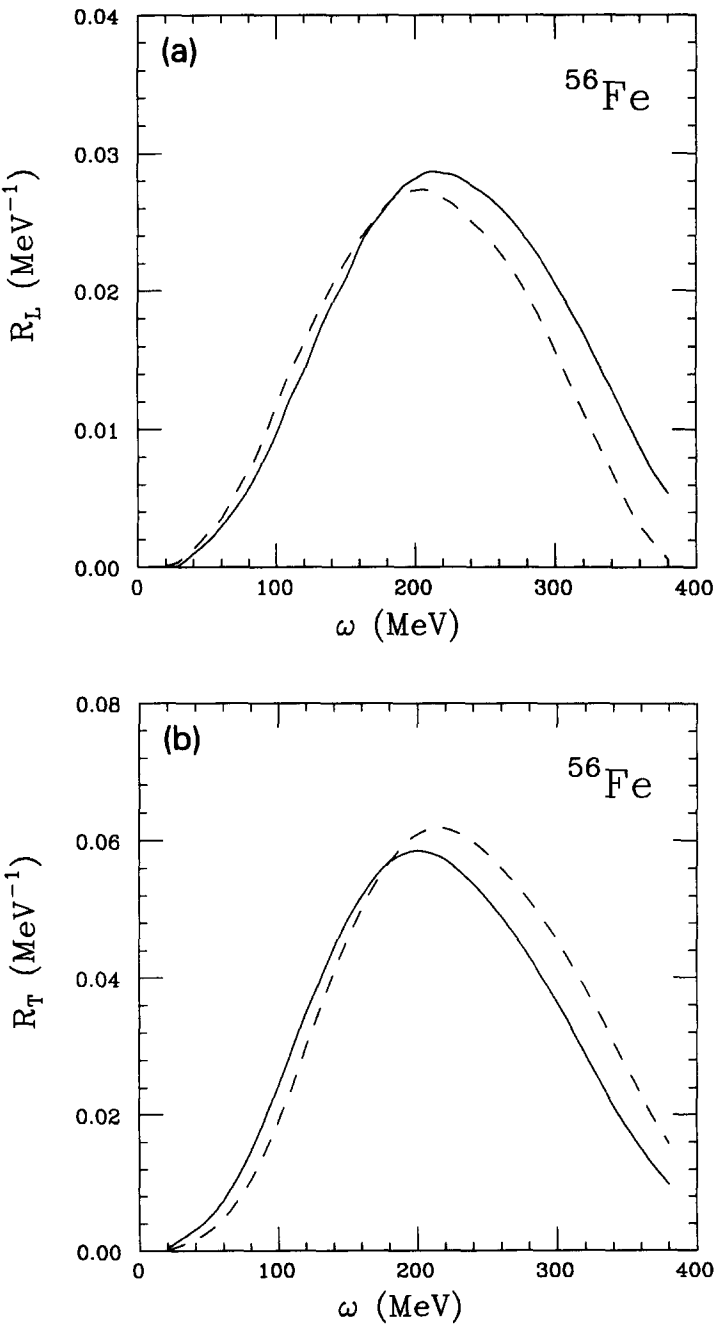

Fig. 4. Comparison of the PWBA-model response functions (solid) with the response functions obtained when the cross sections are calculated in LEMA, but Coulomb effects are ignored in the L/T separation (dash).

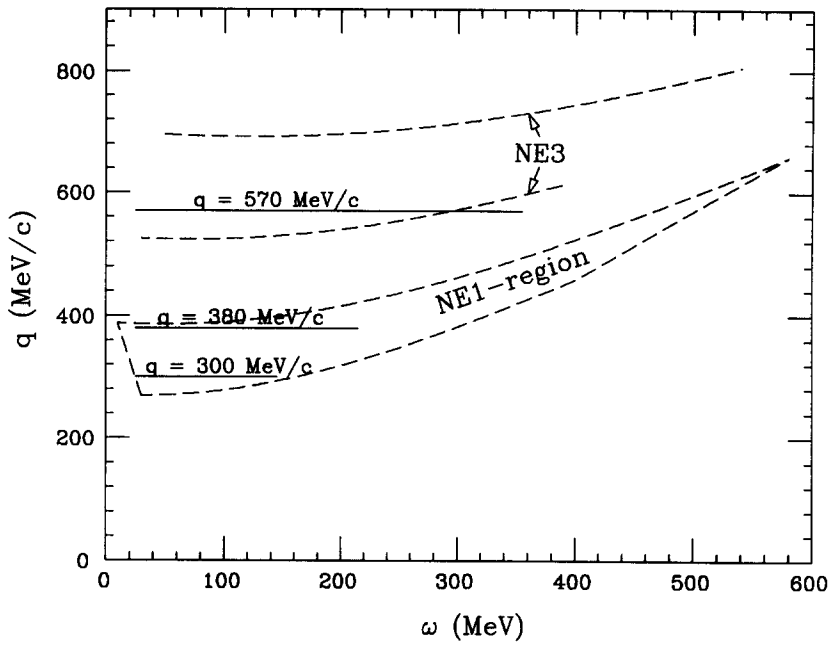

Fig. 5. Kinematics of the SLAC data used in the separation of the world data on ^{12}C and ^{56}Fe. The various lines are described in the text.

For ^{12}C the SLAC data have been combined with an extensive set of data measured at Saclay [7] at scattering angles of 36°, 60°, 90°, and 145°. The kinematical range is similar to the one shown in Fig. 7 for ^{40}Ca. With the measurements done at 36 degrees, the Saclay data alone would allow an L/T separation with quite a large span of ϵ. However, due to the limitations of the incident beam energy the forward-angle data do not cover the high q-region, and thus do not contribute to the determination of $R_L(q,\omega)$ at 570 MeV/c.

The kinematical regions covered by the Bates and the Saclay data on ^{40}Ca are shown in Fig. 6 and 7. The Bates data were measured at scattering angles of 45.5°, 90°, and 140° but only the forward-angle data cover the high q-region. This limits an L/T separation to $q \leqslant 450$ MeV/c if the Bates data alone are used. In the Saclay experiment data were measured at scattering angles of 60°, 90° and 140°. The 90 degree data, however, do not cover the high q-region. The extracted longitudinal response function, which showed the largest suppression of the Coulomb sum at high q, was extracted with two data points only. Systematic errors of uncontrolled origin are particularly dangerous in such a situation where no consistency checks are possible.

For ^{56}Fe the SLAC data can be combined with the data measured at Saclay [9] at identical scattering angles as for the ^{40}Ca data. Data taken at Bates [42] at a scattering angle of 180° have also been included. The data measured at Bates by Altemus et al. [11] could not be used as they were not available in numerical and final form.

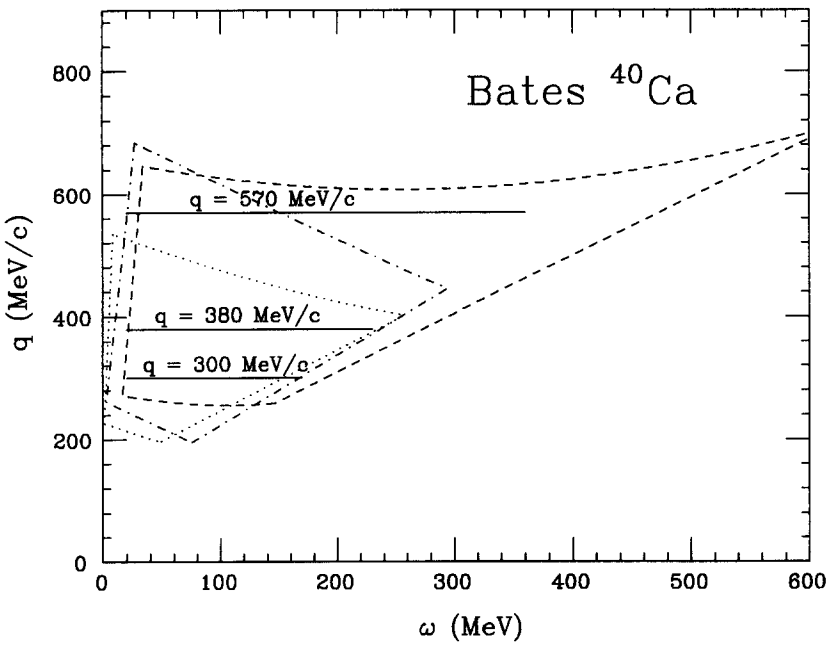

Fig. 6. Kinematics of the Bates ^{40}Ca data. The q–ω regions at 45.5 (dashed), 90 (dots), and 140 degrees (dot–dashed) are shown.

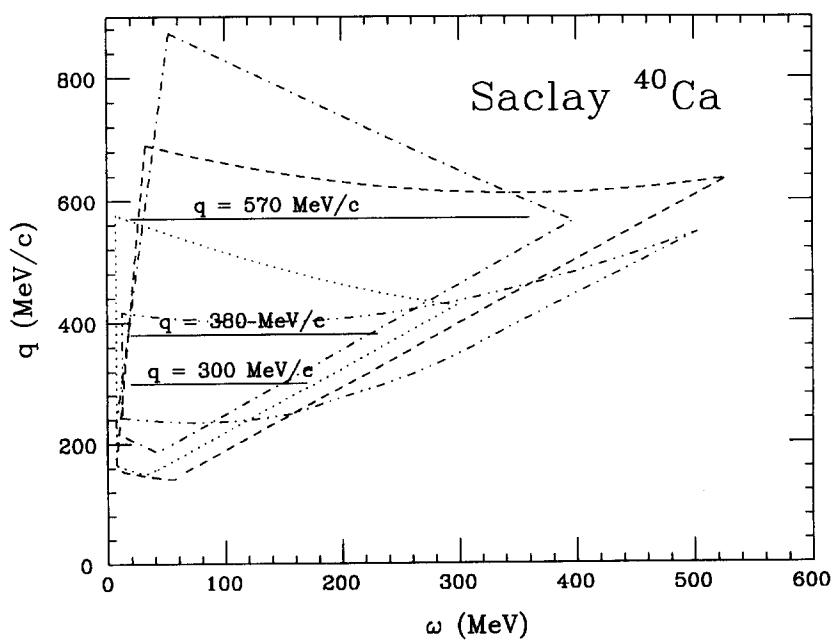

Fig. 7. Kinematics of the Saclay ^{40}Ca data. The q–ω regions at 60 (dashed), 90 (dot), and 140 degrees (dot–dashed) are indicated. The region covered for ^{12}C at 36 degrees is also shown (dot-dot–dashed).

3.2. Systematic errors

As indicated in the introduction experiments which aim for an L/T separation are very sensitive to systematic errors, particularly in kinematic regions at high q and ω where the cross section consists of a small $R_L(q,\omega)$ and a large $R_T(q,\omega)$ component. The subtraction of the large transverse component leads to the well-known blow-up of the uncertainty for the small $R_L(q,\omega)$ component. Using data from one experiment only does not help to avoid these problems as only systematic errors due to the *overall normalization* of the cross section data can be avoided. However, the dominant part of the systematic errors, uncertainties of the spectrometer acceptance, detector efficiencies, background contributions, rescattering, and radiative corrections, are strongly dependent on the specific kinematics. Even for data taken at a single facility they do not cancel in the difference of high-energy/forward-angle and low-energy/backward-angle data.

An important aspect to consider in order to control such energy-dependent effects is the mode in which the data are taken. The experiments performed at SLAC measured data in event-mode data acquisition. For data taken in event-mode data acquisition it is always possible to replay the experiment off-line and use the multi-parameter information from the various detectors to study selectively each event. For the SLAC experiments the redundant detector setup and this mode of data taking allowed for a detailed off-line analysis of energy-dependent effects, and to establish procedures to properly correct the data.

The low-energy experiments mainly measured cross sections in histogram mode, i.e. data were stored in histograms on-line. It was not possible to replay the experiment and study each event separately. As the energy spectra of the scattered electrons are structureless in the quasi-elastic region it is not possible to single out background contributions in the measured histograms.

The significance of energy-dependent effects can best be illustrated by the effects studied during experiment NE1 by Baran et al. and NE9 by Chen et al. [43,44]. Both experiments have been performed with the aim to extract separated response functions from the measured cross sections.

The experiments have been performed at SLAC and have used the 8 GeV/c spectrometer, a QQDDQ spectrometer, to detect the scattered electrons and determine their energy. The detector package consisted of (in the following order) a nitrogen gas threshold Čerenkov detector, ten planes of wire chambers (MWPC) to determine particle trajectories, two planes of plastic hodoscopes, and a segmented lead glass total absorption counter used for particle identification and a redundant energy determination.

The optical properties of the 8 GeV/c spectrometer are such that the track positions at the focal planes were only slightly disturbed by multiple scattering in the preceding Čerenkov mirror, so that the momentum and scattering angle could be reconstructed with good resolution. However, the horizontal interaction point in the target and the out-of-plane angle are most strongly correlated with the *direction* of the track through the wire chambers, so that multiple scattering degraded the resolution with which these quantities were reconstructed. This degradation was a function of E' and affected significantly the

acceptance of the spectrometer, one of the effects to consider in experiments which compare cross sections measured at high and low scattered energy.

Even more important was an excess of low-energy electrons that was observed in both experiments at low E'. These electrons were not rejected with the definition used for a good electron event (valid Čerenkov signal, valid track, away from the edge of the shower counter, acceptable energy signal in the shower counter). The rejection of the background was only possible due to the redundancy of the detector setup which allowed for a second energy determination using the shower counter. At high energy a clean peak in the shower spectrum was found with negligible background at low shower energy. At low E', however, a significant background of low-energy electrons leaking into the peak of good electrons was observed. The contribution showed a systematic energy dependence. Whereas at an energy of 1 GeV it was of the order of only 0.2%, it contributed more than 15% at energies of 0.2 GeV. It was found that a major part of this background was due to electrons which scattered off the yoke and vacuum chamber of the spectrometer magnets.

During the experiment NE9 this background was measured by taking data with an additional collimator which could be inserted between the two dipole magnets of the spectrometer. This collimator reduced the acceptance of the spectrometer by a factor of ~ 2 by blocking events with x–y coordinates far away from the central ray. Data taken for high and low scattered E' were analyzed in an identical way (not subtracting any background in the shower counter spectrum). Cross sections determined with collimator in divided by the ones determined with collimator out were studied as a function of E'.

Whereas the cross section ratios at high energy were consistent with unity, the ratio reached up to 1.2 at low E', indicating a background contribution of $\geqslant 20\%$. This is consistent with the analysis of Baran and the Monte Carlo studies done assuming that the background originates from electrons which had an E' outside the normal acceptance, but reached the detectors after scattering off the yoke of the bending magnets. Because the yoke was only slightly wider than the acceptance region with collimator out, some of the higher E' electrons hit the walls of the vacuum chamber and scattered back into the spectrometer. The Monte Carlo studies confirmed that the collimator was very effective in cutting out most of the background contribution.

The (e, e') experiments performed at Saclay on ^{12}C, ^{40}Ca, and ^{56}Fe, used the "600" spectrometer to detect the scattered electron. This spectrometer was designed to minimize background contributions from events scattered from the yoke. Lead blocks had been installed to prevent electrons with too high energy to scatter from the vacuum chamber and reach the detector system. However, no protection prevented scattering off the side walls of the vacuum chamber covering the pole tips of the spectrometer. In addition the detector setup did not allow for a target position reconstruction in the non-diffractive plane. Studies of an energy-dependent background such as done for the SLAC data could not be done as data were taken in histogram mode. Marchand [45] simulated the pole-tip scattering contribution in the "600" spectrometer for an extended target and found background contributions of up to 13% with variations up to a factor of 2 depending on E'.

In a GEANT simulation with the same assumptions as used by Marchand we could reproduce his background contribution results. We extended the simulation assuming the conditions of the experiments on ^{12}C, ^{40}Ca, and ^{56}Fe. We found background contributions up to 1.3% at low E'. Although it has been shown [46] that a contribution of *only* 5% to the low-energy/backward-angle data would result in a decrease of 20% in the extracted $R_L(q,\omega)$ if only the Saclay data are used, the contribution found in the simulation is too low to explain the suppression of $R_L(q,\omega)$. However, the simulation assumed a perfect geometry and it was found that the background contribution is very sensitive to the overall alignment. A misalignment of the beam position of 2 mm relative to the spectrometer midplane increases the background by a factor of two.

In summary, energy-dependent systematic effects of cross-section data, if not corrected for, lead to suppressed $R_L(q,\omega)$ values. The systematic effects are strongly enhanced in $R_L(q,\omega)$ if only a limited ϵ-range is used in the analysis. This is well known as already the L/T separation performed on ^{56}Fe at Bates [11], the first experiment which provided strongly reduced $R_L(q,\omega)$ values, suffered from such effects. The discovery of secondary scattering contributions from the target chamber aperture and a reanalysis with corrected data significantly increased the $R_L(q,\omega)$ values [9]. The conclusion is further supported by the difference of the results from Bates and from Saclay on ^{40}Ca, and the behaviour of $R_L(q,\omega)$ at high q and ω which shows an (unphysical) negative $R_L(q,\omega)$ just beyond the range of ω usually shown. One must conclude that the only way to reduce the dependence of $R_L(q,\omega)$ on systematic errors is the use of data which cover the entire ϵ-region and the use of event-mode data acquisition.

Future experiments aiming for an improvement of the precision on $R_L(q,\omega)$ should plan for careful studies of energy-dependent effects. The only safe procedure probably will be the measurement of track coordinates after a *fraction* of the deflection by the magnetic dipole field. In this case tracks corresponding to rescattered electrons can unambiguously be identified.

4. Response functions for ^{12}C and ^{56}Fe

Using the world data discussed in the previous section I now determine $R_L(q,\omega)$ and $R_T(q,\omega)$ for ^{12}C and ^{56}Fe.

4.1. Interpolation procedure

The experimental spectra were measured for a given incident energy and scattering angle as a function of the energy loss of the scattered electron, varied by changing the magnetic field of the spectrometer. For an L/T separation, however, one needs cross sections at constant values of q and ω over as large an ϵ-range as possible. To determine such cross sections at a given value of q and ω the data have to be interpolated. This has been done in the past by dividing out the Mott cross section σ_{Mott} to reduce the dominant variation with the incident energy, and by using these reduced cross-section

values to interpolate along lines of constant ω/E to determine the value at a given q and ω. This allows for a reliable interpolation provided data exist with very small spacings in q.

An improved interpolation scheme has been used in the present analysis, as for much of the data, and the NE3 experiment in particular, the required prerequisite of a small spacing in q is not given. Not only σ_{Mott} has been divided out, but also an appropriate sum of elementary electron–nucleon cross sections, i.e. σ_{ep} for the proton and σ_{en} for the neutron. Essentially what is calculated from the data (Fig. 8) is the scaling function $F(y,q)$ defined by [47]

$$F(y,q) = \frac{d^2\sigma}{d\omega d\Omega} \frac{1}{Z\sigma_{ep}(q) + N\sigma_{en}(q)} \frac{d\omega}{dy}. \tag{19}$$

The scaling variable y is given by energy and momentum conservation via

$$y = -q + \sqrt{\omega^2 + 2\omega M}, \tag{20}$$

neglecting small contributions from the binding energy, the perpendicular initial momentum component of the knocked-out nucleon, and the recoil energy of the residual nucleus. The $F(y,q)$ extracted are then used to determine $F(y,q_0)$ at the desired value q_0 by interpolating $F(y,q)$ along lines of constant y.

For $y < 0$ the function $F(y,q)$ is known to be nearly independent of q over a large range of q. This makes the interpolation as reliable as the conventional interpolation scheme even if the data are separated by a large distance in q. For $y > 0$ the dependence of $F(y,q)$ on q is more pronounced as inelastic processes contribute to the cross section. Therefore, the q-value for the L/T separation has been chosen such as to minimize the correction due to the interpolation at large ω (see Figs. 5 and 8). With the choices of q_0 made, the interpolated $F(y,q_0)$ nearly coincide with the measured one, and the calculated changes of $F(y,q)$ due to the interpolation are smaller than the statistical errors, which are at most 10%. Systematic uncertainties of this interpolation scheme are thus of the order of $\leqslant 1\%$.

The interpolation procedure and the subsequent separation has been tested using the data of the Saclay experiments alone. Provided the same interpolation scheme is used (separation along constant ω/E as done traditionally), the published values of $R_L(q,\omega)$ and $R_T(q,\omega)$ [48,49] are reproduced exactly. The improved interpolation scheme, using y-scaling, gives results which are identical within the statistical errors.

4.2. *Experimental results*

The combined world data cover almost the full ϵ-range, with typical values of ϵ ranging from 0.05 to 0.95 for all q-sets. This is to be compared to the low-energy data alone which only cover the region from 0.05 to 0.55. The use of the world data enhances the sensitivity to $R_L(q,\omega)$ by almost a factor of two. The reliability of $R_L(q,\omega)$ is further enhanced by the fact that the additional data, which have the largest weight in

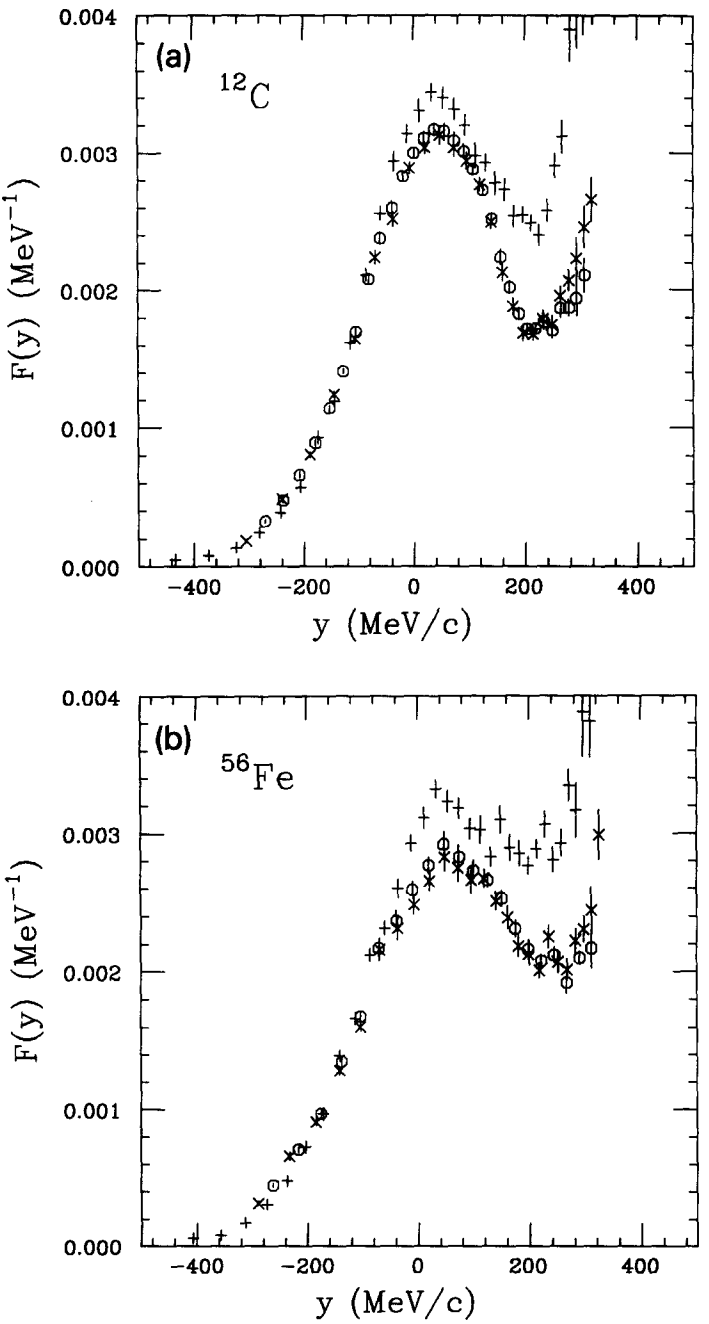

Fig. 8. $F(y, q)$ for the NE3 data. The spectra measured at 15 (×) and 20 degrees (+) are shown together with the interpolated values (○) for ^{12}C (left) and ^{56}Fe (right).

Table 1
Summary of systematic errors of the world data. For the Saclay data between 100 MeV $< E' <$ 200 MeV a systematic error is assumed which rises linearly from 3.7% to 5.3% with decreasing E'

	^{12}C	^{56}Fe
SLAC NE3 [26]	3.5%	3.5%
SLAC NE1 [28]	3.2%	3.2%
Saclay $E' > 200$ MeV [7,46]	3.7%	3.7%
Saclay $E' < 200$ MeV [7,46]	3.7–5.3%	3.7–5.3%
Bates [42]		5.0%

determining $R_L(q,\omega)$ since measured at forward angle, are the data taken in event-mode, i.e. the most reliable ones (see Subsection 3.2).

In the analysis of the world data the systematic errors of the various data sets are added in quadrature to the statistical ones after the interpolation procedure is performed. The systematic errors used are summarized in Table 1. They slightly differ for the Saclay data [50] from the values used in the previous analysis [51], without significantly changing the results.

Typical examples of the L/T separation of the world data are presented in Fig. 9, where the results are compared to a separation using the Saclay data alone. In particular for ^{56}Fe the world data yield values for $R_L(q,\omega)$ which are systematically higher than the ones obtained when using low-energy data alone. Note that in the analysis of the low-energy data alone the statistical errors only have been used.

To illustrate the origin of this difference two Rosenbluth plots at $q = 570$ MeV/c are shown in Fig. 10 for $\omega = 85$ and 305 MeV. A linear fit to all data (the low-energy data) is shown with the solid (dashed) line. The data at low ω are very consistent. However, there is a systematic trend observable in the high ω-region (represented by the $\omega = 305$ MeV plot). The slopes, which determine the $R_L(q,\omega)$ values, are significantly increased when the high-energy data are included in the fit. At $\omega = 305$ MeV the dashed line misses the SLAC data point by 14% (more than 4 standard deviations of the systematic error of the SLAC data).

4.3. Theoretical results

In Fig. 11 the complete set of $R_L(q,\omega)$ for ^{12}C and ^{56}Fe is shown and compared to two model calculations. The solid lines represent the results of the state-of-the-art microscopic nuclear matter calculation by Fabrocini and Fantoni [16] mentioned in the introduction. These authors solve the many-body Schrödinger equation for nuclear matter in the framework of the orthogonal version of correlated basis function theory [52]. In the Hamiltonian realistic two- and three-body nucleon interactions are taken into account. The calculation starts with uncorrelated Fermi-gas model wave functions and generates a set of correlated states using a correlation operator which has the same structure as the nucleon–nucleon interaction. The calculation accounts for dynamical short-range nucleon–nucleon correlations up to 2p2h terms for both the initial and final

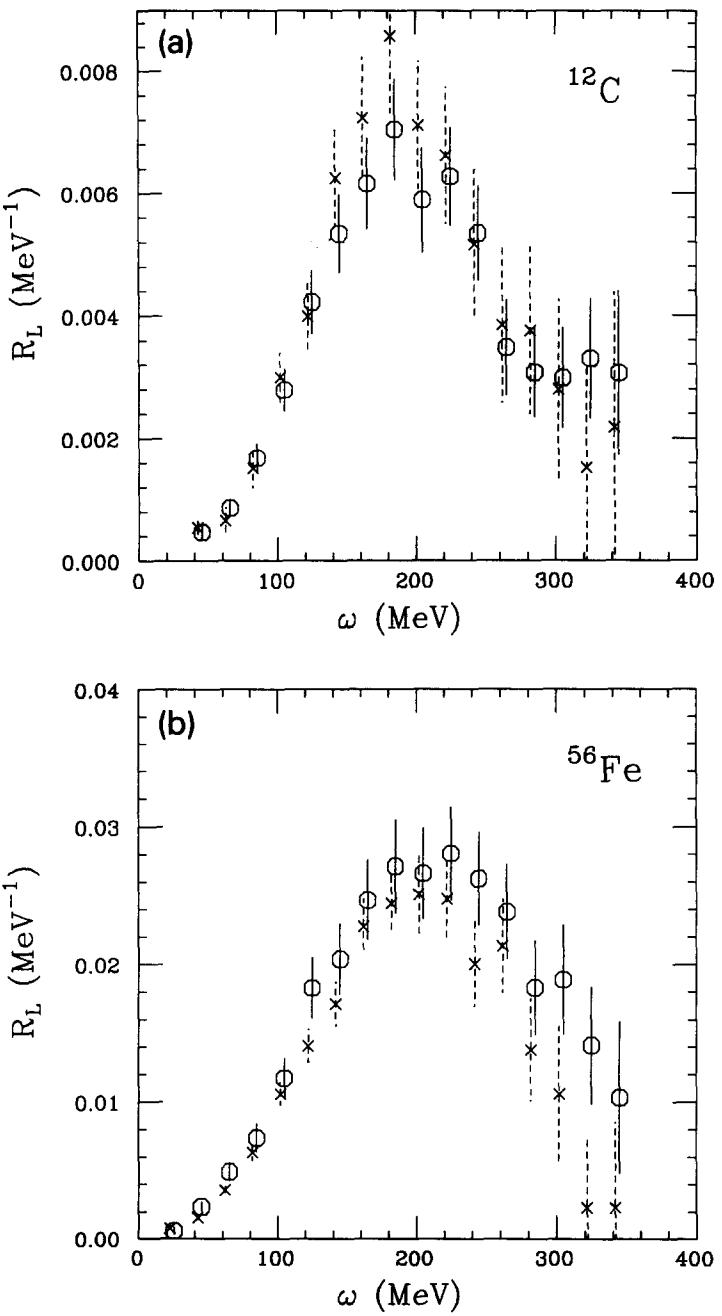

Fig. 9. $R_L(q,\omega)$ at $q = 570$ MeV/c obtained using the world data (o), or using the data of Barreau et al. [7] (Meziani et al. [9]) on ^{12}C(^{56}Fe) only (×). To clearly distinguish the error bars of the two data sets the binning of the (o) data has been shifted by 3 MeV with respect to the (×) data.

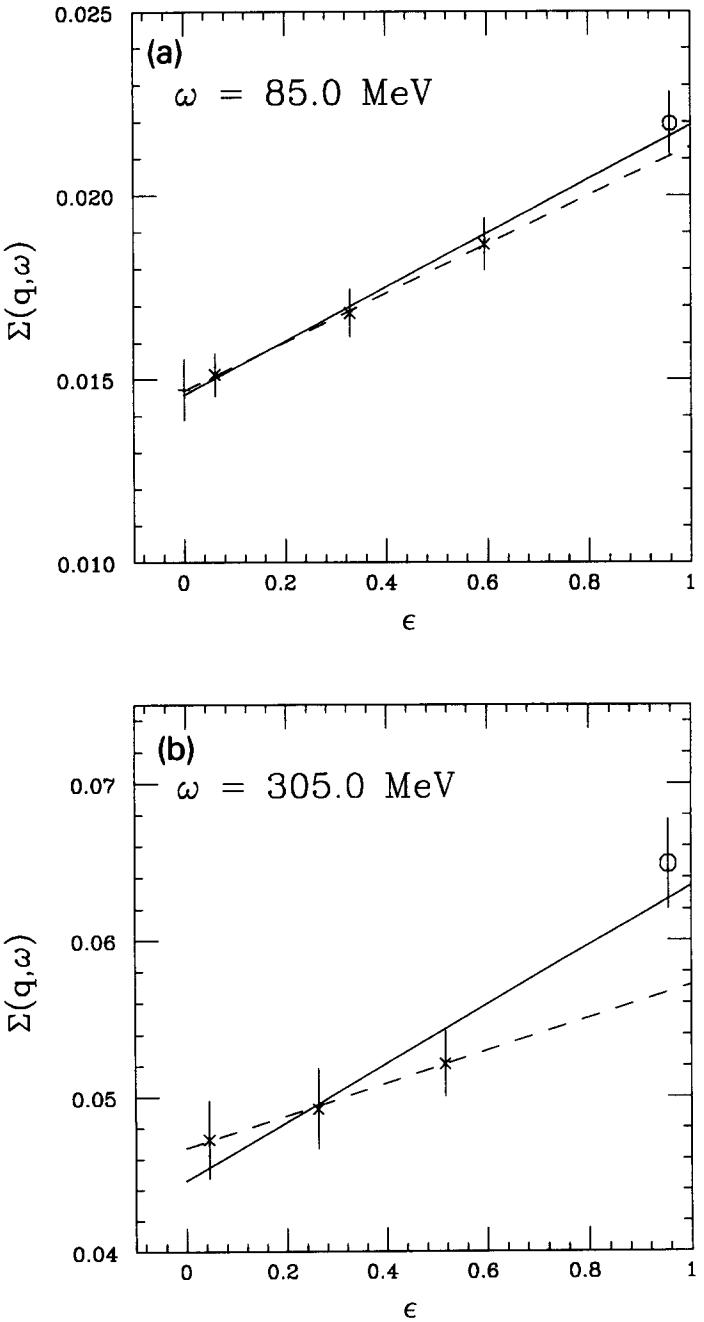

Fig. 10. Representative Rosenbluth plots for ^{56}Fe at q = 570 MeV/c. The data points of Day et al. [26], Meziani et al. [9] and Hotta et al. [42] are indicated with ○, × and +, respectively. $R_L(q,\omega)$ is the slope of a fit using all data (solid) or using the Saclay data alone (dashed). Note the suppressed zero.

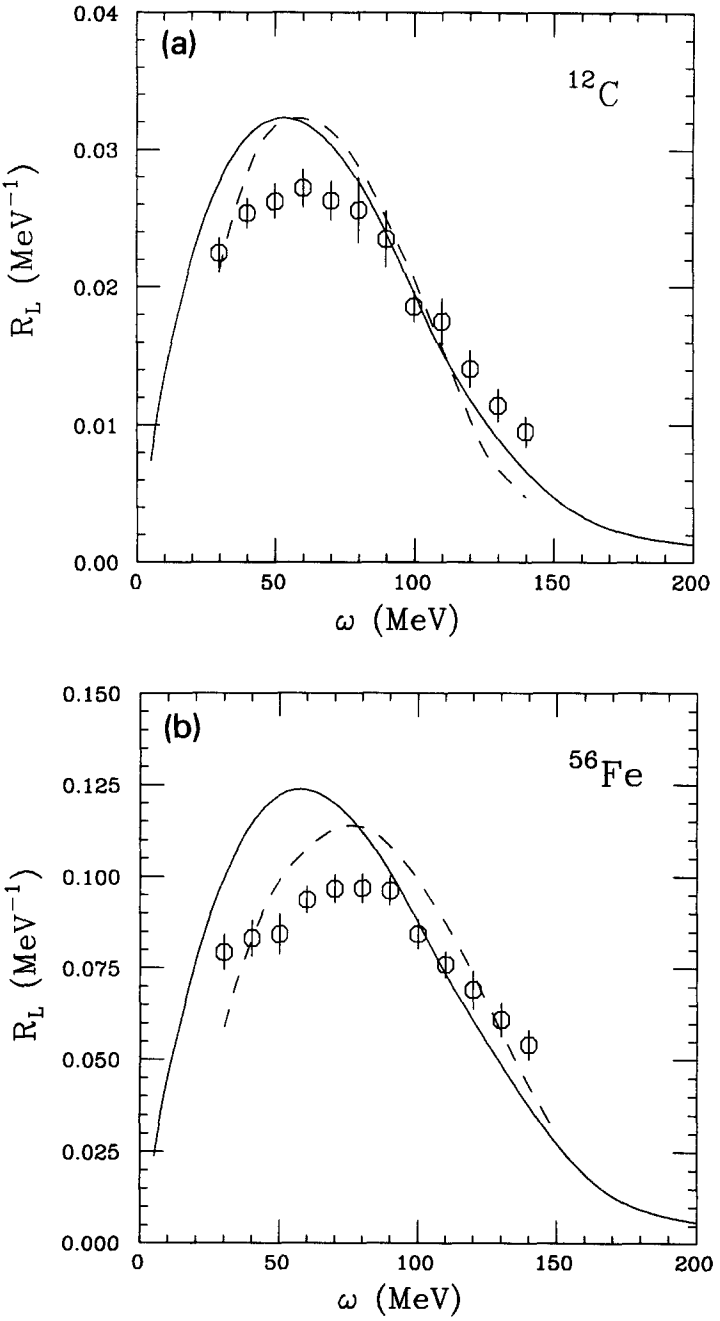

Fig. 11. Results on $R_L(q,\omega)$ at q = 300, 380 and 570 MeV/c obtained using the world data, compared to the calculations of Fabrocini et al. (solid) and Jin et al. (dashed).

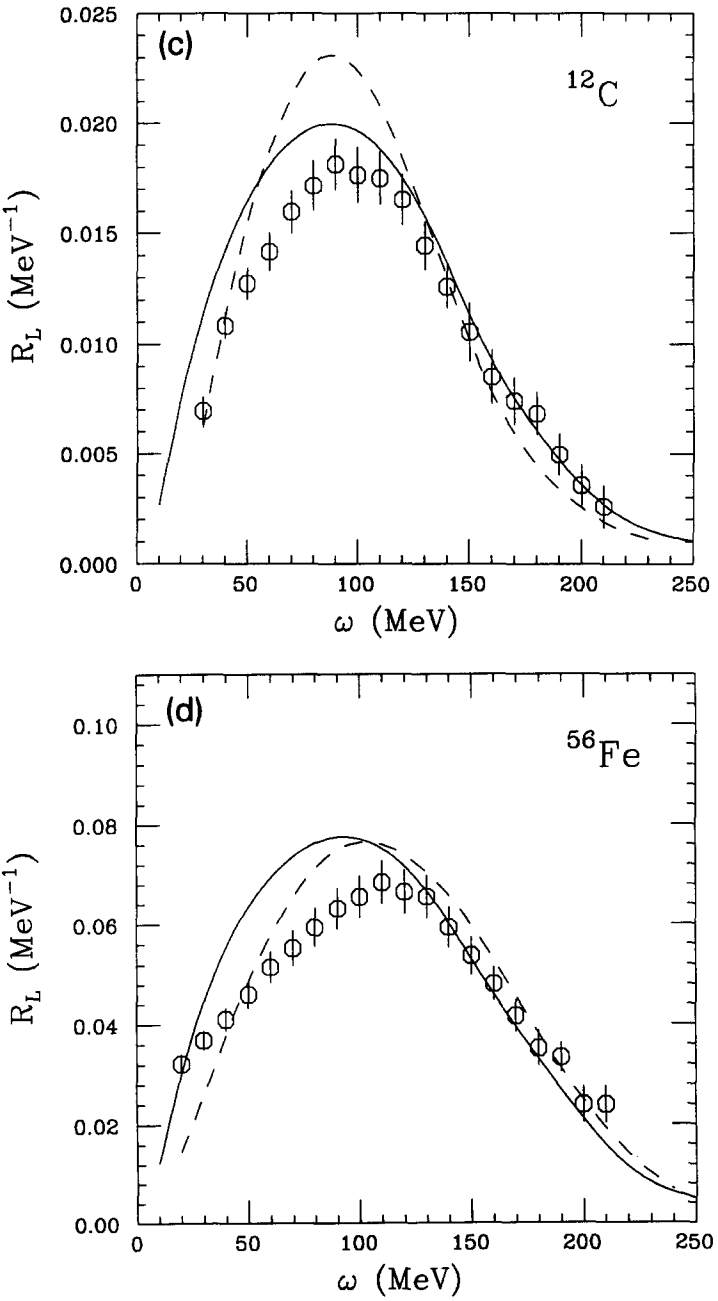

Fig. 11 — continued.

states.

The reduced density of finite nuclei has been taken into account using the local density approximation (LDA) [53] for the response functions. The response functions are calculated for 0.25, 0.5, 0.75 and 1.0 times the nuclear matter density. Using a

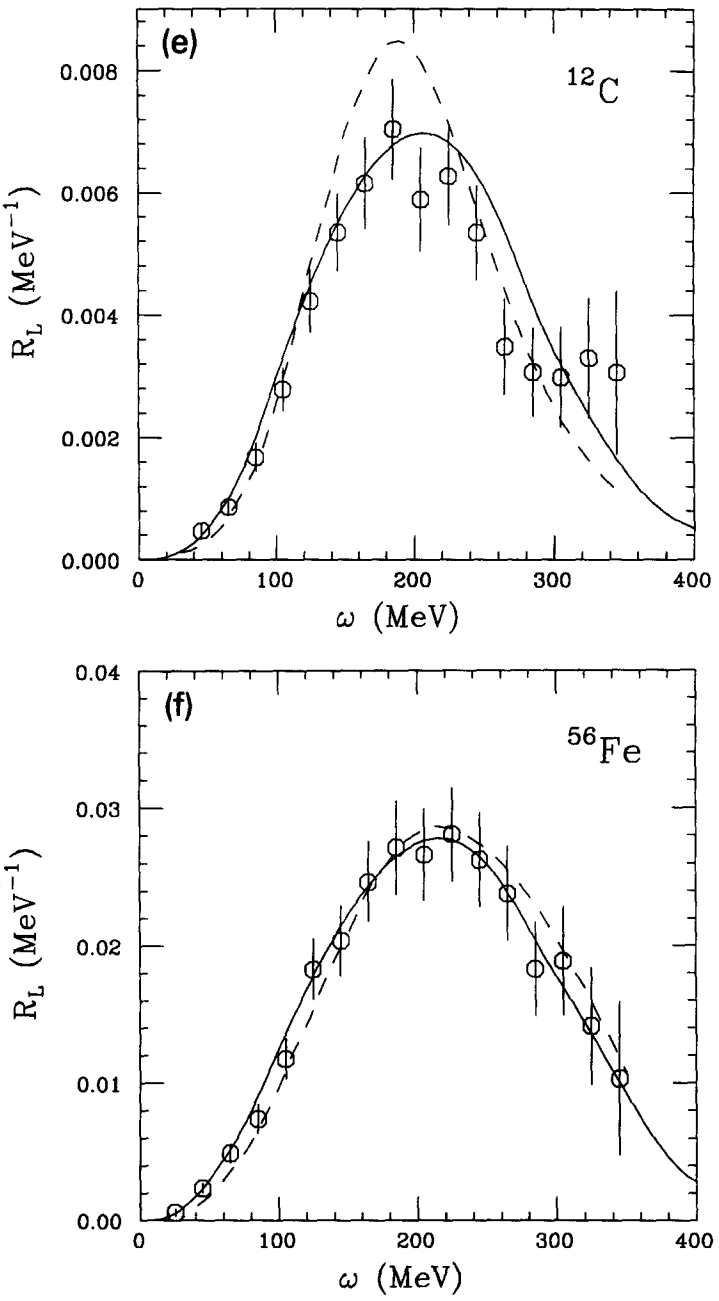

Fig. 11 — continued.

3pF fit [54] to the density the fraction of nucleons in ^{12}C and ^{56}Fe falling into the corresponding bins in density are determined and used to calculate the response functions for the finite nuclei. As can be seen in Fig. 11 very good agreement of the calculation is obtained for $R_L(q,\omega)$ at $q = 570$ MeV/c. The fact that the results are too high for

the lower q-values is not surprising as the LDA is not a good approximation when Pauli correlations are significant and restrict the nuclear phase space probed.

The dashed line represents the single-particle calculation by Jin et al. [32] who derive nuclear wave functions for the bound and the continuum states using a relativistic Hartree model. In this calculation the cross section is an incoherent sum of single-nucleon knock-out contributions from occupied states. The knocked-out nucleon does not necessarily leave the nucleus without further interaction. However, since the subsequent interactions do not affect the (e, e') cross sections, the potential used does not contain an absorptive part. The free Dirac current operator was used in these calculations, and the bound and continuum nucleon wave functions were solutions to the Dirac equation with scalar and vector potentials calculated in the relativistic Hartree model. The results of this model are generally too high in comparison to the data, an observation already made in Ref. [23].

For completeness we also present in Fig. 12 the results for the transverse response functions $R_T(q, \omega)$, and we also compare them to the calculations discussed above. In both calculations only the quasi-elastic contribution to the total strength is derived, meson exchange currents and Δ-excitation are not accounted for. However, for a conclusive comparison with data on the *transverse* response these degrees of freedom need to be taken into account. While the tail of the Δ adds incoherently and increases the response at large ω, meson-exchange currents add *coherently* to the one-body current. Amaro et al. [55] calculated the transverse response for ^{12}C and ^{40}Ca including the pionic, the seagull and the Δ-terms. This calculation yields a shift of the $R_T(q, \omega)$ peak towards lower ω and a *reduction* of the strength ($\sim 5\%$ on the peak) due to two-body currents. Such a shift qualitatively seems to be confirmed by the data.

5. Response functions for ^{40}Ca

As indicated in the introduction, the consistency of the experimental data on ^{40}Ca is particularly unsatisfactory. In the q-range from 300 MeV/c to 450 MeV/c the recent analysis by Yates et al. [23] yields a longitudinal response function which is much larger than the one found by Meziani et al. [9]. Given this inconsistency and the fact that the result of Meziani for ^{40}Ca gives apart from ^{208}Pb the lowest Coulomb sum for all nuclei, an analysis of the combined world data is particularly interesting.

None of the SLAC experiments measured (e, e') cross section data on ^{40}Ca. However, for the SLAC kinematics, data for ^{40}Ca can reliably be interpolated from the data on other nuclei.

5.1. *Interpolation to ^{40}Ca*

In [56] we described in detail how response functions for nuclear matter can be extracted from the SLAC data on finite nuclei using an appropriate extrapolation procedure. It was shown that, in LDA, the cross section per nucleon is expected to be a linear function of $A^{-1/3}$. Experimentally, it was found by Day et al. that indeed the cross

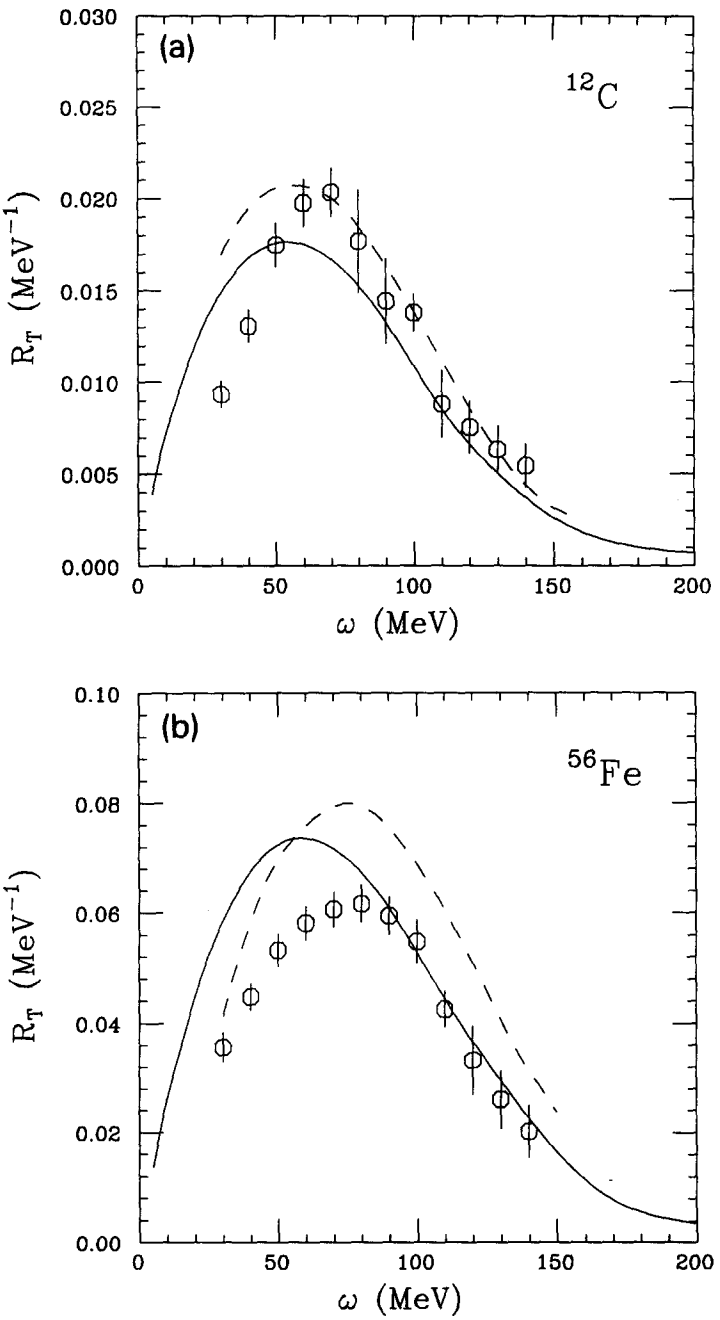

Fig. 12. Results on $R_T(q,\omega)$ at q = 300, 380 and 570 MeV/c obtained using the world data, compared to the calculations of Fabrocini et al. (solid) and Jin et al. (dashed).

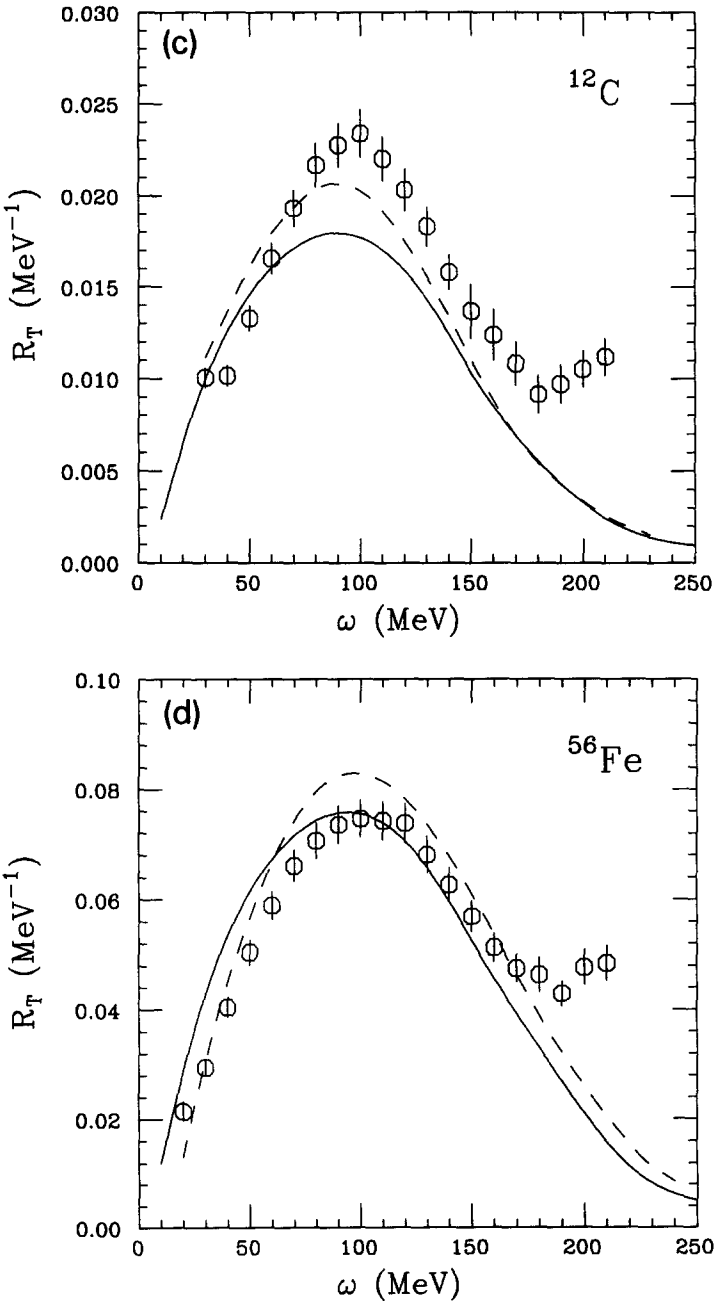

Fig. 12 — continued.

sections at all q, ω could be represented as a linear function of $A^{-1/3}$ for nuclei with mass number $A = 12$, 27, 56, and 197. For the kinematics of the SLAC data, the linear dependence on $A^{-1/3}$ therefore is an established experimental fact. As a consequence of this $A^{-1/3}$ dependence, it is possible to extract the high-energy response function for

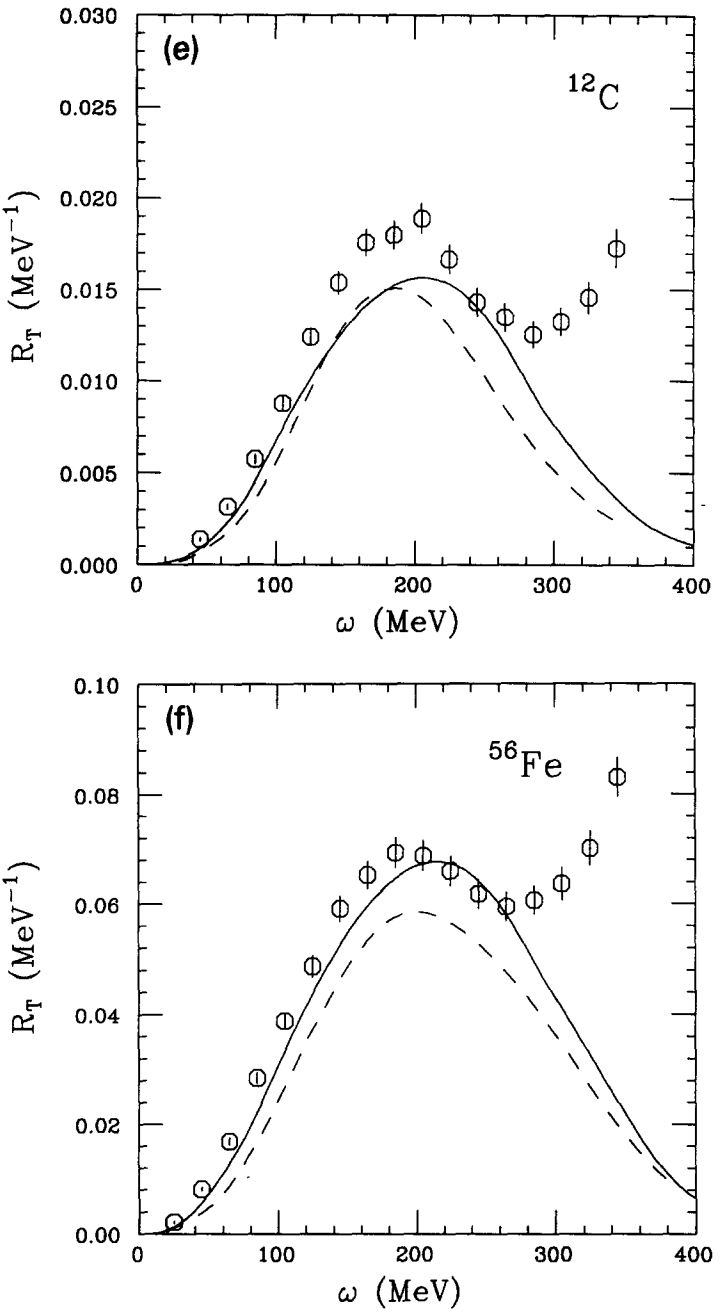

Fig. 12 — continued.

^{40}Ca via an interpolation to $40^{-1/3}$ starting from the data on ^{27}Al.

In [56] we explained that the interpolation of the response can be done in two slightly different ways. For the total response the cross section $\sigma(q,\omega)$ can be divided by A and plotted as a function of $A^{-1/3}$:

$$S(q,\omega) = \sigma(q,\omega)/A\,. \tag{21}$$

Alternatively, if inelastic contributions are removed from the response (or are negligible) one can use the additional knowledge that the response function is dominated by the quasi-elastic scattering process. For quasi-elastic scattering, the relative contribution of protons and neutrons changes as a function of A. Although the contribution of the protons dominate due to the larger ep cross section, the contribution of the neutrons is not negligible. An interpolation to $N = Z = 20$ using nuclei with a N/Z ratio different from 1 then can be performed with the following function:

$$S(q,\omega) = \sigma(q,\omega)\frac{(\sigma_{ep}+\sigma_{en})}{2(Z\sigma_{ep}+N\sigma_{en})}\,, \tag{22}$$

where σ_{ep} and σ_{en} are the elastic electron–proton and electron–neutron cross sections, respectively. The second approach takes into account the fact that generally $N \neq Z$, in particular for ^{56}Fe, but neglects the fact that this approach is not valid for inelastic contributions.

Half of the average difference of the resulting ^{40}Ca(e,e') cross sections obtained using the two approaches—2.7%(1.8%) for the Baran et al. (Day et al.) data—is taken as an additional contribution to the systematic error.

For the two low q-points of the SLAC experiment the ^{12}C and ^{56}Fe cross sections have been used in the interpolation as described above. For the high q-point (the one of main interest to the question of the CSR) a slightly different approach has been taken. At this kinematics data are available for A = 12, 27, 56, and 197; these data determine with considerable redundancy the slope of a linear fit to the data. The fitted slope together with the ^{27}Al(e,e') data is used to get the ^{40}Ca cross sections. In this way the interpolated ^{40}Ca data depend on the results of ^{197}Au,^{56}Fe and ^{12}C only to the degree to which these data influence the slope.

5.2. Results for $R_L(q,\omega)$ and $R_T(q,\omega)$

The same procedure as for ^{56}Fe and ^{12}C has been used to determine the separated response functions from the combined world cross section data on ^{40}Ca. The treatment of the systematic errors is identical to the treatment used for the ^{56}Fe and the ^{12}C data. The systematic errors used for the ^{40}Ca data are summarized in Table 2.

Examples of the L/T separation are presented in Fig. 13 where they are compared to separations using data from single experiments. One should note that both low-energy experiments have been analyzed in the identical way as the combined data, except for the fact that in Fig. 13 the systematic errors of the cross sections have not been included for the low-energy data, such as to be able to compare to the published results.

At the lower q-value, 380 MeV/c, the separation can be compared to both the Saclay and the Bates results. From the analysis of Yates et al. it is known that the Bates and Saclay results disagree. Yates extracted a much higher integrated strength from the Bates data. Thus, it is not surprising that the result of the present analysis, obtained by

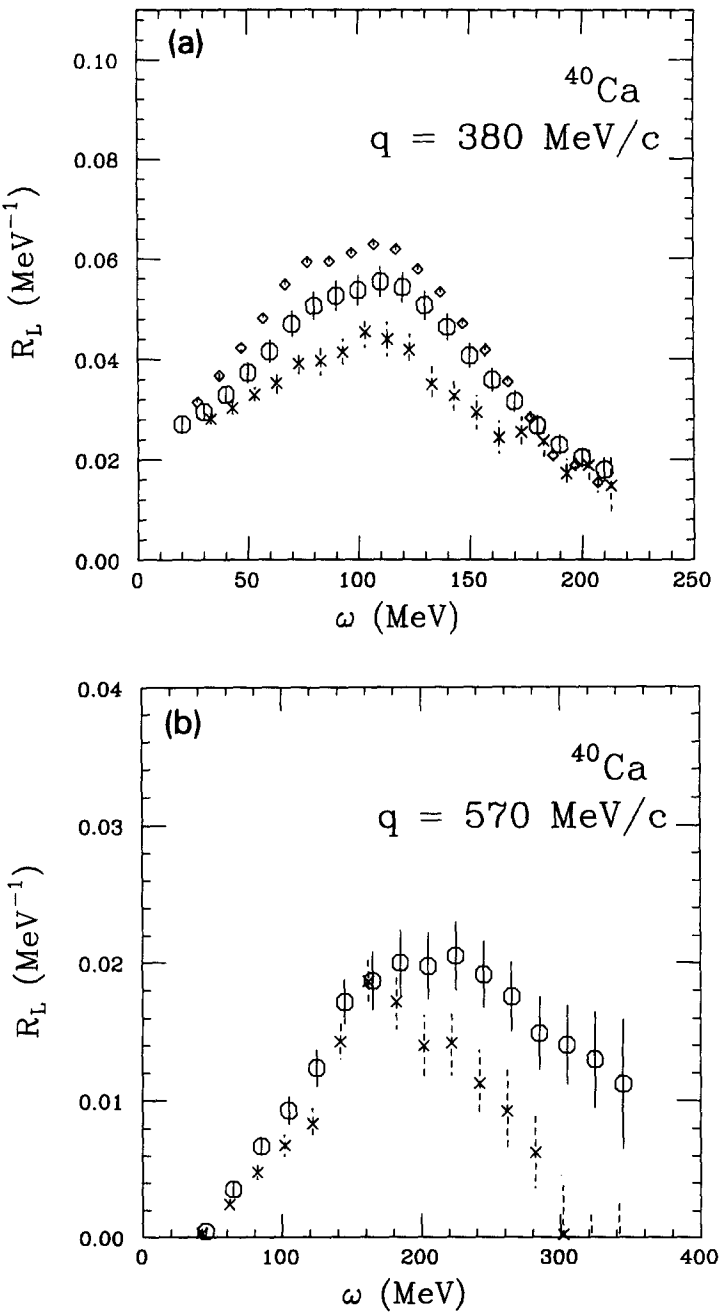

Fig. 13. Results on $R_L(q,\omega)$ for ^{40}Ca at q = 380 MeV/c (left) and q = 570 MeV/c (right). The results obtained using the world data (○) are compared to the results using the data of Saclay alone (×), or the data of Bates alone (◇).

Table 2
Summary of systematic errors of the world data on ^{40}Ca. For the Saclay data between 100 MeV $< E' <$ 200 MeV a systematic error is assumed which rises linearly from 3.7% to 5.3% with decreasing E'

	^{40}Ca
Interpolated from [26]	3.9%
Interpolated from [28]	4.2%
Saclay $E' > 200$ MeV [7,46]	3.7%
Saclay $E' < 200$ MeV [7,46]	3.7–5.3%
Bates [23]	4.0%

combining the world data, gives $R_L(q,\omega)$ values which are in between the two low-energy results. It should be emphasized, however, that the present result is not simply an average of two sets of inconsistent data; the longitudinal strength is much better determined by the additional SLAC data.

Whereas the Saclay data are internally consistent when considering statistical errors alone, the Bates data give large χ^2 in the Rosenbluth fits, indicating the importance of systematic errors. If the systematic errors are added in quadrature, as done in the analysis of the world data, the results using the Bates data alone are much more in line with the results of the world data and give reasonable χ^2's in the Rosenbluth fits. Neglecting systematic errors leads to the large $R_L(q,\omega)$ values because the forward-angle data point, being high in value, has a much lower statistical error than the more backward angle data.

At $q = 570$ MeV/c $R_L(q,\omega)$ from the world data can only be compared to the Saclay result [9] as only *one* set (45.5 degree) of the Bates data covers this high q-value. For ^{40}Ca we find similar results as for ^{56}Fe. The world data yield values of $R_L(q,\omega)$ which are systematically higher than the ones obtained when using low-energy data alone. The discrepancy is larger than the discrepancy for ^{56}Fe. This might be attributed to the fact that the Saclay $R_L(q,\omega)$ for ^{40}Ca has been determined with only two ϵ-values, which increases the sensitivity to systematic errors. Two Rosenbluth plots at $q = 570$ MeV/c are shown in Fig. 14 for $\omega = 85$ MeV and 305 MeV to illustrate these points. A linear fit to all data (the Saclay data) is shown with the solid (dashed) line. Again at low ω the data are quite consistent. However, the same systematic trend as for the ^{56}Fe data is observable in the high ω-region (represented by the $\omega = 305$ MeV plot). The dashed line misses the SLAC data point by 25% which is more than 5 standard deviations, where the error includes *both* the systematic error of the data and the systematic error due to the interpolation.

Figs. 15 and 16 show the complete set of $R_L(q,\omega)$ and $R_T(q,\omega)$ for ^{40}Ca. They are compared to the two calculations discussed in the previous section. The solid lines again correspond to the results of the microscopic nuclear matter calculation by Fabrocini and Fantoni [16]. The dashed lines represent the results from the single-particle calculation by Jin et al. [32]. The same trend can be observed as for $R_L(q,\omega)$ and $R_T(q,\omega)$ of ^{56}Fe and ^{12}C. Whereas good agreement of the calculation is obtained for $R_L(q,\omega)$ at $q = 570$ MeV/c, the theoretical results are too high for the lower q-values where Pauli correlations are important.

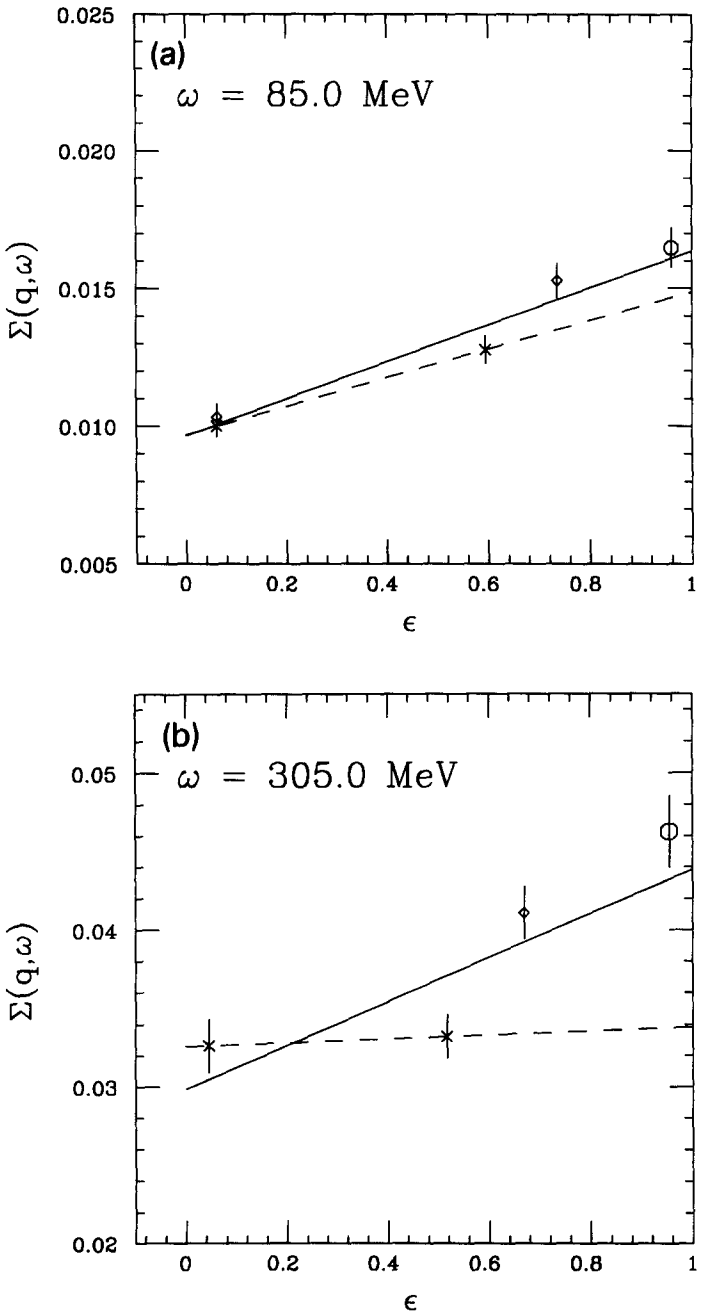

Fig. 14. Rosenbluth plots for ^{40}Ca at $q = 570$ MeV/c. The interpolated data point of Day et al. [26], the data points of Meziani et al. [9] and Yates et al. [23] are indicated with ○, × and ◇, respectively. $R_L(q,\omega)$ is the slope of a fit to all data (solid) and to the Saclay data alone (dashed). Note again the suppressed zero.

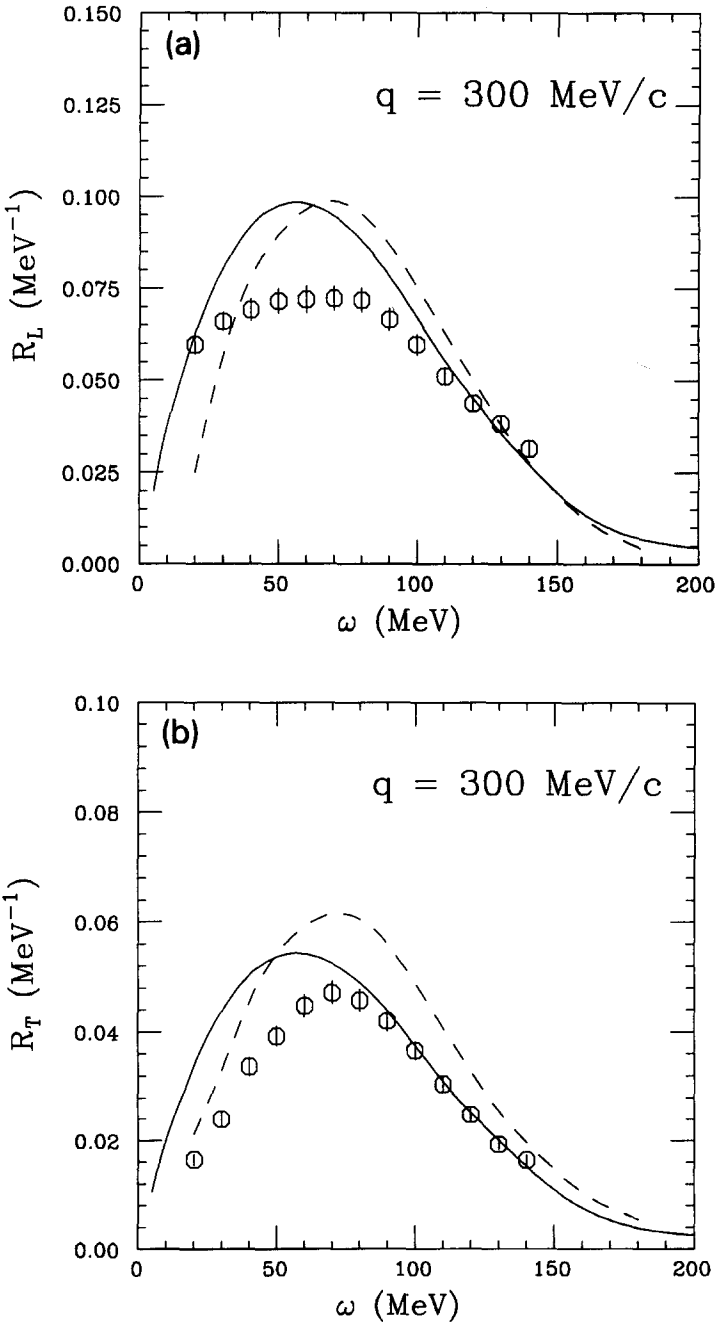

Fig. 15. Results on $R_L(q,\omega)$ and $R_T(q,\omega)$ for ^{40}Ca at 300 MeV/c obtained using the world data. The experimental results are compared to the calculations of Fabrocini et al. (solid) and Jin et al. (dashed).

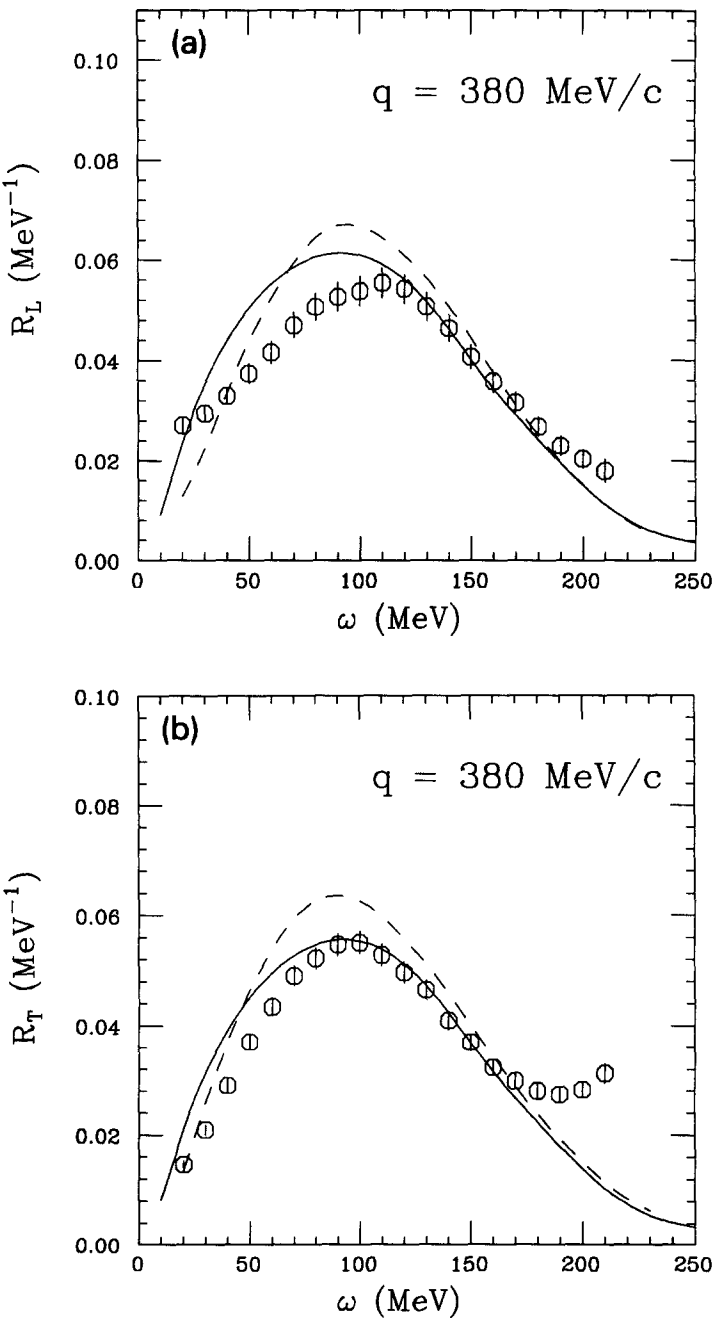

Fig. 16. Results on $R_L(q,\omega)$ and $R_T(q,\omega)$ for ^{40}Ca at 380 and 570 MeV/c obtained using the world data compared to the calculations of Fabrocini et al. (solid) and Jin et al. (dashed).

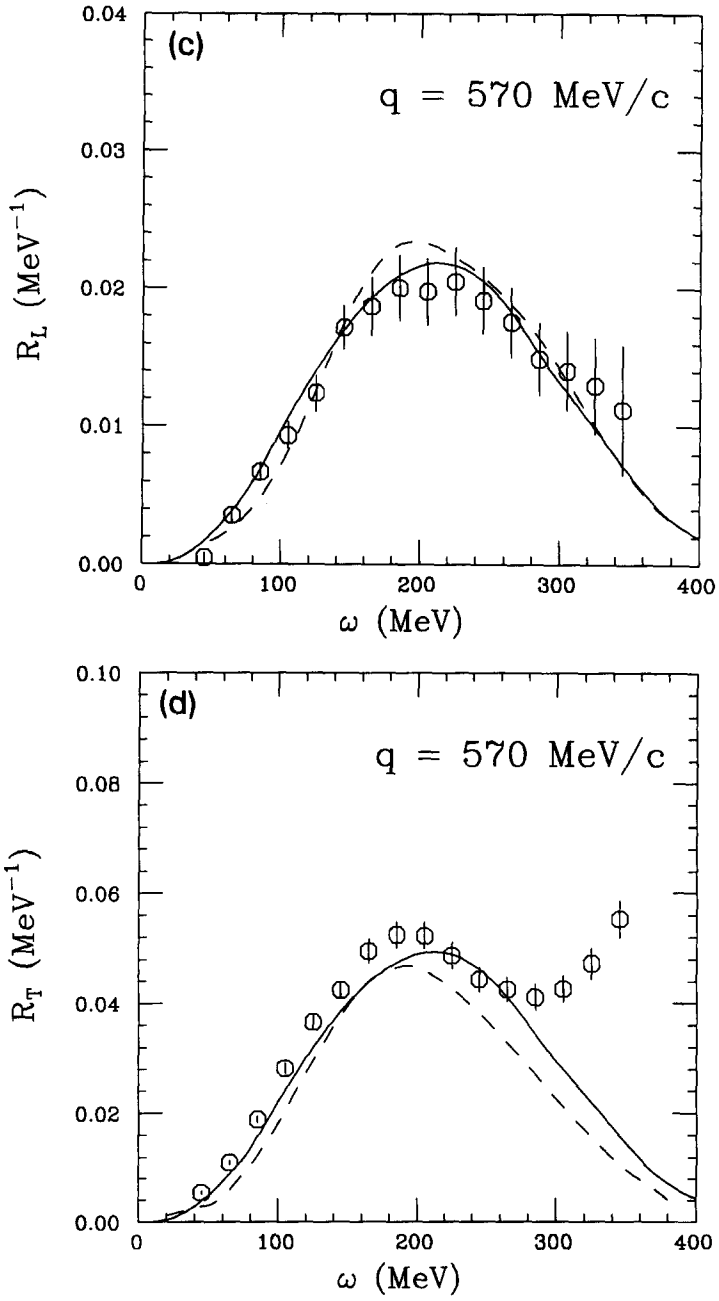

Fig. 16 — continued.

6. Determination of the Coulomb sum

The experimental longitudinal response functions can now be used to determine the Coulomb sum experimentally. A number of issues have to be considered if one aims

at testing the CSR experimentally. The CSR as defined in Eq. (1) is derived in a non-relativistic framework, it assumes point-like protons, and $R_L(q,\omega)$ is integrated from $\omega+$ to ∞. However, with electron scattering $R_L(q,\omega)$ can only be measured over the space-like region $\omega \leqslant q$. In practice, due to the large background and the large radiative corrections at large ω, not even the limit $\omega = q$ can be reached. In addition, protons are extended objects whose size has to be taken into account. Although the charge form factor of the neutron is small, its contribution has to be considered as well. In the q-region most interesting for a test of the CSR relativity might play a role.

The following quantity is used below to determine the Coulomb sum from the data:

$$S_L^{\omega_{\max}}(q) = \frac{1}{Z}\int_{\omega+}^{\omega_{\max}} d\omega \frac{R_L(q,\omega)}{\tilde{G}_e(Q^2)^2}\,. \tag{23}$$

After factoring out an appropriate nucleon charge form factor $\tilde{G}_e^2(Q^2)$, which accounts for the finite size and relativistic effects, the longitudinal response $R_L(q,\omega)$ is integrated from ω_+ to $\omega_{\max}$, the maximal energy loss covered by the data. Also used below is the quantity $S_L(q)$ defined as in Eq. (23), but replacing $\omega_{\max}$ with infinity.

6.1. *Correlation effects and finite* $\omega_{\max}$

Given that only the space-like ω-region is accessible with electron scattering, $S_L(q)$ only reaches 1 for $q \to \infty$ when the entire strength is contained in the space-like region. As pointed out before, the data on $R_L(q,\omega)$ that determine the experimental longitudinal sums do not even cover the entire space-like region. Thus, part of the missing strength in the data is due to a shift of strength to higher ω-values. This strength is not predicted by the Fermi-gas model. Dynamical short-range correlations, due to repulsive and tensor nucleon–nucleon forces, provide such a mechanism and it was estimated [16,57–60] that they give a significant contribution to the strength in the unmeasured ω-region.

Schiavilla et al. [59] proposed a parameterization of the high-ω "tail contribution" to $R_L(q,\omega)$ which satisfies the energy-weighted sum rule. A significant contribution was found in the tail which, when added to the experimental sum, almost satisfied the Coulomb sum (within the large error bars of the experimental results). However, the missing strength in ^{40}Ca could not be accounted for, and data from SLAC [27] suggested that the tail contribution is smaller than estimated by Schiavilla et al.

As these phenomenological extrapolations of the tail are not entirely satisfactory, we here use a calculation that, due to the inclusion of short-range correlations in both the initial and final states, contains the physics responsible for the appearance of this tail. In the present work, we integrate the theoretical $R_L(q,\omega)$ values from Fabrocini and Fantoni [16] from $\omega_{\max}$ to infinity to obtain the strength for $\omega > \omega_{\max}$.

6.2. Finite-size effects

To account for the finite size of the nucleons the appropriate nucleon charge form factor $G_e(Q^2)$ has to be divided out before the experimental $R_L(q,\omega)$ values are integrated over. To take into account the contribution of electron–neutron scattering, the following relation can be employed:

$$G_e^2(Q^2) = G_{ep}^2(Q^2) + \frac{N}{Z} G_{en}^2(Q^2)\,. \tag{24}$$

Z and N are the numbers of protons and neutrons in the nucleus, $G_{ep}(Q^2)$ and $G_{en}(Q^2)$ the corresponding charge form factors for which the parameterizations of Simon et al. [61] and Galster et al. [62] are used in the present work.

Once scattering from the neutron is taken into account, the energy loss dependence of the matrix element that determines $R_L(q,\omega)$ can not be eliminated by dividing out the squared proton form factor [63]; one is left with an expression that contains the ratio $G_{en}(Q^2)/G_{ep}(Q^2)$ which depends on ω. Consequently, closure can not be applied in the derivation of the CSR. However, Benhar also showed that the effect is small for the q-range considered in this work. In fact, the contribution of neutrons using the above parameterization for the neutron form factor is at most 1.3% at the highest q of 570 MeV/c.

6.3. Relativistic effects

As the Coulomb sum rule is formulated in a non-relativistic framework, relativistic corrections have to be considered. An approach to incorporate relativistic effects while keeping the original flavor of the sum rule was proposed by de Forest [14]. He considered relativistic effects as corrections to the non-relativistic currents. To order $1/M^2$ the only correction to the charge density operator comes from the Darwin–Foldy term [13]. The effect on $S_L(q)$ may be included by multiplying $S_L(q)$ with an appropriate factor (see Ref. [14]). Higher-order terms are unspecified, but an approach to include them was proposed by Friar [64] in the context of elastic scattering. His result was used in the calculation of the Coulomb sum by de Forest and states that relativistic corrections are incorporated by replacing the effective form factor in Eq. (24) by

$$\tilde{G}_e^2(Q^2) = \left(G_{ep}^2(Q^2) + \frac{N}{Z} G_{en}^2(Q^2)\right) \frac{1 + Q^2/4M^2}{1 + Q^2/2M^2}. \tag{25}$$

I will use this expression for the effective form factor in the analysis of data. It has been argued by de Forest [14] that the ambiguity of the higher-order terms is small and that the sum rule with the above relation again approaches 1 in the high q-limit.

An alternative way to study relativistic effects is accessible when using relativistic models. Walecka [65] was the first to study the CSR in a relativistic quantum field theory based on baryons and mesons. His result for the longitudinal response integrated up to infinity diverged in the high q-limit due to inclusion of $N\overline{N}$-pair production in the

one-body term. Matsui [66] separated the contributions to the sum rule into a space-like term accessible with electron scattering and a time-like term. He showed that excitations of the Fermi sea (N-scattering) are found entirely in the space-like region, while $N\bar{N}$-pair production is found entirely in the time-like region. Neglecting contributions from the magnetic moments his result for the *space-like* sum rule in the high q-limit has a value of $Z/2$. The difference to the non-relativistic result, which is shifted into the time-like region, is interpreted by Matsui as the Pauli correlation between the Fermi nucleons and the Dirac sea nucleons.

This result was later confirmed by DoDang [67] and was further discussed by Chinn et al. [68]. In a relativistic approach the Dirac plane waves contain the normalization factor $N_D = ((E+m)/2E)^{1/2}$. In the non-relativistic limit $N_D^2 \to 1$, whereas relativistically $N_D^2 \to 1/2$. This simply reflects the fact that the positive energy states span only half of the relativistic Hilbert space. Note that this phase-space effect is accounted for in the prescription of de Forest. The correction factor in Eq. (25), which accounts for relativistic effects, has a value of 2 in the high q-limit. It thus compensates the phase-space effect and recovers the non-relativistic limit. Although this correction factor of de Forest is somewhat model dependent it accounts accurately for relativistic effects for $\leqslant 1$ GeV [68].

In a relativistic approach the anomalous magnetic moments of the nucleons modify the charge density operator and contribute to the sum rule. Calculations of the sum rule including the anomalous magnetic moments have been done by DoDang et al. [67] and by Donnelly et al. [69] within the relativistic Fermi-gas model, and more recently by Ferrée et al. [70]. The results of Ferrée et al. suggest that the de Forest prescription might be overestimating relativistic corrections by at most 3% of the sum-rule value for the q-values relevant to this paper.

6.4. *Results for the Coulomb sum*

The results for the experimental $S_L^{\omega_{max}}(q)$ are summarized in Table 3. The statistical errors of $S_L^{\omega_{max}}(q)$ have been treated in the standard way using the statistical errors of the cross-section data. The systematic errors are accounted for by changing the cross-section data of each set by their systematic error, and redetermining $S_L^{\omega_{max}}(q)$. The effects of the systematic errors on $S_L^{\omega_{max}}(q)$ of the different experiments have been added in quadrature. The resulting error represents the dominant contribution of the total error. The statistical errors, of order 1–3% (depending on q), and a 2% error for the uncertainty of the proton form factor, give only small contributions to the total error. The neutron contribution to the sum is $\leqslant 1.3\%$ at all q. Thus, despite the large uncertainty of the neutron form factor, the contribution to the error is negligible. In Table 3 the total errors of $S_L^{\omega_{max}}(q)$ are given.

The present values are up to a factor of 1.6 higher than previous determinations of Coulomb sums. In addition, the error bars are smaller by up to a factor of two.

I now discuss the results for the Coulomb sum rule at the highest q (570 MeV/c) where Pauli correlations are the smallest, and where an interpretation in terms of a

Table 3
Results of the Coulomb sums using the world data. The systematic errors are included

q (MeV/c)	ω_{max} (MeV)	$S_L^{\omega_{max}}(q)$ for ^{12}C	$S_L^{\omega_{max}}(q)$ for ^{40}Ca	$S_L^{\omega_{max}}(q)$ for ^{56}Fe
300	145	0.69±0.03	0.63±0.03	0.62±0.03
380	215	0.78±0.04	0.81±0.04	0.80±0.06
570	355	0.88±0.13	0.91±0.15	0.91±0.12

Table 4
Results for the Coulomb sum at $q = 570$ MeV/c for ^{56}Fe

	$S_L(q)$
Result of [71]	0.60 ± 0.20
Dipole G_{ep} replaced by [61]	0.64 ± 0.21
Relativistic correction added	0.69 ± 0.23
SLAC data added	0.86 ± 0.12
Coulomb correction added	0.91 ± 0.12
Tail contribution added	0.97 ± 0.12

model-independent sum rule makes sense. Integrating the strength of the theory [16] up to the experimental ω_{max} gives a theoretical value $S_L^{\omega_{max}}(570) = 0.91$. This result for the Coulomb sum is in *complete agreement* with the experimental result for all nuclei considered. No "quenching" in the data is observed.

An estimate of the contribution to $S_L(q)$ from $\omega > \omega_{max}$ can be obtained by an empirical fit of $R_L(q,\omega) \propto (\omega/\omega_{max})^{\lambda}$ to the last few data points. The fit gives a contribution of 0.07 to the sum for ^{12}C and ^{56}Fe and of 0.10 for ^{40}Ca. Extending the integration of the theory over the entire space-like region yields $S_L(570) = 0.97$. The 3% difference between $S_L(570)$ and 1 is explained by short-range correlations.

Adding the tail contribution determined from the theory, the experimental result of the Coulomb sum $S_L(570)$, 0.94 ± 0.13 for ^{12}C, 0.97 ± 0.15 for ^{40}Ca, and 0.97 ± 0.12 for ^{56}Fe is completely satisfied within errors. This conclusion does not change if the relativistic correction given by de Forest is indeed overestimated by 0.03 as discussed by Ferrée et al. Within errors the Coulomb sums allow for the reduction of 0.03 relative to 1 due to the dynamical correlations discussed above.

In order to illustrate the effects of the different ingredients in the determination of the Coulomb sum for ^{56}Fe I summarize in Table 4 the different contributions leading from the "quenching of 40%" of the Coulomb sum to the "unquenched" result found in this work. The first line gives the result of Ref. [71], obtained using the Saclay data, the dipole proton form factor and neglecting relativistic and Coulomb corrections. The following lines give the sum when adding consecutively the various effects.

It is obvious that more than one half of the difference between Ref. [71] and 1 is due to approximations that were not justified (dipole form factor, missing relativistic effects, improper treatment of Coulomb effects, omission of the tail contribution). Adding the

data most sensitive to $S_L(q)$ (the SLAC data) changes $S_L(q)$ by only 18%, a change that is smaller than the total error of the non-SLAC data!

7. Conclusions

In this paper I performed an analysis of the response functions for ^{12}C, ^{40}Ca, and ^{56}Fe, using the world data on inclusive quasi-elastic scattering. The longitudinal and the transverse response functions have been determined at q-values of 300, 380 and 570 MeV/c.

The use of the world data—a standard procedure in the determination of precise form factors [61,72–75]—enhances the sensitivity to $R_L(q,\omega)$ by a factor of two compared to previous results and allows for a more reliable determination of $R_L(q,\omega)$ with smaller systematic errors. Since $R_L(q,\omega)$ is mainly determined by the inclusion of the high-energy/forward-angle data, the inclusion of data covering a larger range in energy makes the results less dependent on the use of the maximum range of scattered energies as imposed by measurements using a single facility. It has been demonstrated that near the bottom of their useful energy range spectrometers are subject to systematic errors due to rescattering effects. Only the event-mode data acquisition performed for the case of high-energy/small-angles allows for a reliable control of such energy-dependent effects. Such a careful check of the data is a prerequisite for experiments that aim for a reliable L/T separation.

In extracting the response functions, Coulomb distortion has been corrected using the Local-EMA approach developed by Wright et al. The LEMA is in much better agreement with the full DWBA calculation than the approaches used in the past. Such a proper treatment of the Coulomb distortion is also important in a determination of the Coulomb sum at very high q. The seemingly low Coulomb sum determined by Chen et al. [44] at $q = 1.1$ GeV/c is mainly due to an improper treatment of the Coulomb distortion using the simple EMA approach.

The results for $R_L(q,\omega)$ and $R_T(q,\omega)$ are compared to a theoretical calculation which includes consistently short-range nucleon–nucleon correlations in both the initial and final states. The longitudinal response functions are in complete agreement with this calculation. The "quenching", which has been one of the long-standing problems of nuclear physics, is absent.

The results of $R_L(q,\omega)$ have been used to determine the Coulomb sum which is most interesting at the highest q-value where Pauli correlation effects are negligible and where one would expect saturation. In the determination of the Coulomb sum the most recent parameterization of the nucleon charge form factors have been used and relativistic corrections have been included. The strength in the unmeasured space-like region has been determined from the nuclear matter calculation. The experimental results of the Coulomb sum for ^{12}C, ^{40}Ca and ^{56}Fe are in *complete agreement* with conventional expectations. As one would expect, the determined results saturate the Coulomb sum at the highest q-value at the value of one. No A-dependent quenching is observed and no

exotic effects like swollen nucleons are needed to explain the data.

The challenge for the future will be a determination of the Coulomb sum with systematic errors reduced by about a factor of 3. Only then can one come back to the original interest in the Coulomb sum, the use of the *deviation from one* as a measure for short-range correlations in nuclei.

References

[1] R.R. Whitney, I. Sick, J.R. Ficenec, R.D. Kephart and W.P. Trower, Phys. Rev. C 9 (1974) 2230.
[2] E.J. Moniz, I. Sick, R.R. Whitney, J.R. Ficenec, R.D. Kephart and W.P. Trower, Phys. Rev. Lett. 26 (1971) 445.
[3] C. Marchand, P. Barreau, M. Bernheim, P. Bradu, G. Fournier, Z.E. Meziani, J. Miller, J. Morgenstern, J. Picard, B. Saghai, S. Turck-Chieze, P. Vernin and M.K. Brussel, Phys. Lett. B 153 (1985) 29.
[4] K.A. Dow, S. Dytman, D. Beck, A. Bernstein, I. Blomqvist, H. Caplan, D. Day, M. Deady, P. Demos, W. Dodge, G. Dodson, M. Farkondeh, J. Flanz, K. Giovanetti, R. Goloskie, E. Hallin, E. Knill, S. Kowalski, J. Lightbody, R. Lindgren, X. Maruyama, J. McCarthy, B. Quinn, G. Retzlaff, W. Sapp, C. Sargent, D. Skopik, I. The, D. Tieger, W. Turchinetz, T. Ueng, N. Videla, K. vonReden, R. Whitney and C. Williamson, Phys. Rev. Lett. 61 (1988) 1706.
[5] S.A. Dytman, A.M. Bernstein, K.I. Blomqvist, T.J. Pavel, B.P. Quinn, R. Altemus, J.S. McCarthy, G.H. Mechtel, T.S. Ueng and R.R. Whitney, Phys. Rev. C 38 (1988) 800.
[6] K.F. von Reden, C. Alcorn, S.A. Dytman, B. Lowry, B.P. Quinn, D.H. Beck, A.M. Bernstein, K.I. Blomqvist, G. Dodson, K.A. Dow, J. Flanz, G. Retzlaff, C.P. Sargent, W. Turchinetz, M. Farkondeh, J.S. McCarthy, T.S. Ueng and R.R. Whitney, Phys. Rev. C 41 (1990) 1084.
[7] P. Barreau, M. Bernheim, J. Duclos, J.M. Finn, Z. Meziani, J. Morgenstern, J. Mougey, D. Royer, B. Saghai, D. Tarnowski, S. Turck-Chieze, M. Brussel, G.P. Capitani, E. de Sanctis, S. Frullani, F. Garibaldi, D.B. Isabelle, E. Jans, I. Sick and P.D. Zimmermann, Nucl. Phys. A 402 (1983) 515.
[8] M. Deady, C.F. Williamson, J. Wong, P.D. Zimmermann, C. Blatchley, J.M. Finn, J. LeRose, P. Sioshansi, R. Altemus, J.S. McCarthy and R.R. Whitney, Phys. Rev. C 28 (1983) 631.
[9] Z. Meziani, P. Barreau, M. Bernheim, J. Morgenstern, S. Turck-Chieze, R. Altemus, J. McCarthy, L.J. Orphanos, R.R. Whitney, G.P. Capitani, E. de Sanctis, S. Frullani and F. Garibaldi, Phys. Rev. Lett. 52 (1984) 2130.
[10] M. Deady, C.F. Williamson, P.D. Zimmermann, R. Altemus and R.R. Whitney, Phys. Rev. C 33 (1986) 1897.
[11] R. Altemus, A. Cafolla, D. Day, J.S. McCarthy, R.R. Whitney and J.E. Wise, Phys. Rev. Lett. 44 (1980) 965.
[12] S.D. Drell and C.L. Schwartz, Phys. Rev. 112 (1958) 568.
[13] K.W. McVoy and L. Van Hove, Phys. Rev. 125 (1962) 1034.
[14] T. de Forest, Jr., Nucl. Phys. A 414 (1984) 347.
[15] G. Orlandini and M. Traini, Rep. Prog. Phys. 54 (1991) 257.
[16] A. Fabrocini and S. Fantoni, Nucl. Phys. A 503 (1989) 375.
[17] J.V. Noble, Phys. Rev. Lett. 46 (1981) 412.
[18] L.S. Celenza, A. Harindranath and C.M. Shakin, Phys. Rev. C 33 (1986) 1012.
[19] P.J. Mulders, Nucl. Phys. A 459 (1986) 525.
[20] H. Kurasawa and T. Suzuki, Phys. Lett. B 208 (1988) 160.
[21] R.D. McKeown, Phys. Rev. Lett. 56 (1986) 1452.
[22] I. Sick, Lecture Notes in Physics 260 (1986) 42.
[23] T.C. Yates, C.F. Williamson, W.M. Schmitt, M. Osborn, M. Deady, P.D. Zimmerman, C.C. Blatchley, K.K. Seth, M. Sarimento, B. Parker, Y. Jin, L.E. Wright and D.S. Onley, Phys. Lett. B 312 (1993) 382.
[24] A. Zghiche, J.F. Daniel, M. Bernheim, M.K. Brussel G.P. Capitani, E. de Sanctis, S. Frullani, A. Gerard, J.M. Goff, A. Magnon, C. Marchand, Z.E. Meziani, J. Morgenstern, J. Picard, D. Reffay-Pikeroën, M. Traini, S. Turck-Chieze and P. Vernin, Nucl. Phys. A 572 (1994) 513.
[25] C. Blatchley, J. LeRose, O.E. Pruet, P.D. Zimmermann, C.F. Williamson and M. Deady, Phys. Rev. C 34 (1986) 1243.

[26] D. Day, J.S. McCarthy, Z.E. Meziani, R. Minehart, R. Sealock, S.T. Thornton, J. Jourdan, I. Sick, B.W. Filippone, R.D. McKeown, R.G. Milner, D.H. Potterveld and Z. Szalata, Phys. Rev. C 48 (1993) 1849.
[27] D.T. Baran, B.F. Filippone, D. Geesaman, M. Green, R.J. Holt, H.E. Jackson, J. Jourdan, R.D. McKeown, R.G. Milner, J. Morgenstern, D.H. Potterveld, R.E. Segel, P. Seidl, R.C. Walker and B. Zeidman, Phys. Rev. Lett. 61 (1988) 400.
[28] D.T. Baran, The Electroproduction of the Delta Isobar in Nuclei, PhD thesis, Northwestern University, 1989.
[29] D.H. Potterveld, A Measurement of inclusive quasi-elastic electron scattering at high momentum transfer., PhD thesis, California Institute of Technology, 1989.
[30] J.D. Bjorken and S.D. Drell (McGraw-Hill, New York, 1964).
[31] H. Überall, Electron scattering from complex nuclei (Academic Press, New York, 1971).
[32] Y. Jin, D.S. Onley and L.E. Wright, Phys. Rev. C 45 (1992) 1311.
[33] Y. Jin, D.S. Onley and L.E. Wright, Phys. Rev. C 50 (1994) 168.
[34] F. Lenz and R. Rosenfelder, Nucl. Phys. A 176 (1971) 513.
[35] D.R. Yennie, F.L. Boos and D.G. Ravenhall, Phys. Rev. B 137 (1965) 882.
[36] R. Rosenfelder, Ann. of Phys. 128 (1980) 188.
[37] J. Knoll, Nucl. Phys. A 223 (1974) 462.
[38] M. Traini, S. Turck-Chieze and A. Zghiche, Phys. Rev. C 38 (1988) 2799.
[39] M. Traini and M. Covi, Preprint, 1994.
[40] Y. Jin and L.E. Wright, private communication, 1994.
[41] L.E. Wright et al., to be published, 1996.
[42] A. Hotta, P.J. Ryan, H. Ogino, B. Parker, G.A. Peterson and R.P. Singhal, Phys. Rev. C 30 (1984) 87.
[43] J.P. Chen, The longitudinal and transverse response functions in $^{56}Fe(e,e')$ at Q^2 near 1 $(GeV/c)^2$, PhD thesis, University of Virginia, 1990.
[44] J.P. Chen, Z.E. Meziani, G. Boyd, L.M. Chinitz, D.B. Day, L.C. Dennis, G. Dodge, B.W. Filippone, K.L. Giovanetti, J. Jourdan, K.W. Kemper, T. Koh, W. Lorenzon, J.S. McCarthy, R.D. McKeown, R.G. Milner, R.C. Minehart, J. Morgenstern, J. Mougey, D.H. Potterveld, O.A. Rondon-Aramayo, R.M. Sealock, L.C. Smith, S.T. Thornton, R.C. Walker and C. Woodward, Phys. Rev. Lett. 66 (1991) 1283.
[45] C. Marchand, Etude des fonctions de reponse electromagnetiques et des distributions en moment des protons de grande impulsion dans le noyau d'helium-3 par diffusion inelastique d'electrons., PhD thesis, Universite de Paris-Sud, 1987.
[46] Z.E. Meziani, Etude des fonctions de reponse transverse et longitudinale en diffusion profondement inelastique d'electrons sur les noyaux ^{40}Ca, ^{48}Ca et ^{56}Fe., PhD thesis, Universite de Paris-Sud, 1984.
[47] D. Day, J.S. McCarthy, Z.E. Meziani, R. Minehart, R. Sealock, S.T. Thornton, J. Jourdan, I. Sick, B.W. Filippone, R.D. McKeown, R.G. Milner, D.H. Potterveld and Z. Szalata, Phys. Rev. Lett. 59 (1987) 427.
[48] P. Barreau, M. Bernheim, J. Duclos, J.M. Finn, Z. Meziani, J. Morgenstern, J. Mougey, D. Royer, B. Saghai, D. Tarnowski, S. Turck-Chieze, M. Brussel, G.P. Capitani, E. de Sanctis, S. Frullani, F. Garibaldi, D.B. Isabelle, E. Jans, I. Sick and P.D. Zimmermann, Note CEA-N-2334, (1983).
[49] Z. Meziani, P. Barreau, M. Bernheim, J. Morgenstern, S. Turck-Chieze, R. Altemus, J. McCarthy, L.J. Orphanos, R.R. Whitney, G.P. Capitani, E. de Sanctis, S. Frullani and F. Garibaldi, Rapport DPh-N/Saclay no 2292, 1985.
[50] J. Morgenstern, private communication, 1995.
[51] J. Jourdan, Phys. Lett. B 353 (1995) 189.
[52] S. Fantoni and V.R. Pandharipande, Nucl. Phys. A 473 (1987) 234.
[53] O. Benhar, A. Fabrocini, S. Fantoni and I. Sick, Nucl. Phys. A 579 (1994) 493.
[54] H. de Vries, C.W. de Jager and C. de Vries, Nuclear and Atomic Data Tables 36 (1987) 495.
[55] J.E. Amaro, G. Co and A.M. Lallena, Nucl. Phys. A 578 (1994) 365.
[56] D. Day, J.S. McCarthy, Z.E. Meziani, R. Minehart, R.M. Sealock, S. Thornton, J. Jourdan, I. Sick, B.W. Filippone, R.D. McKeown, R.G. Milner, D. Potterveld and Z. Szalata, Phys. Rev. C 40 (1989) 1011.
[57] M. Cavinato, D. Drechsel, E. Fein, M. Marangoni and A.M. Saruis, Nucl. Phys. A 423 (1984) 376.
[58] G. Orlandini and M. Traini, Phys. Rev. C 31 (1985) 280.
[59] R. Schiavilla, D.S. Lewart, V.R. Pandharipande, S.C. Pieper, R.B. Wiringa and S. Fantoni, Nucl. Phys. A 473 (1987) 267.
[60] G. Co, K.F. Quader, R.D. Smith and J. Wambach, Nucl. Phys. A 485 (1988) 61.
[61] G.G. Simon, Ch. Schmitt, F. Borkowski and V.H. Walter, Nucl. Phys. A 333 (1980) 381.

[62] S. Galster, H. Klein, J. Moritz, K.H. Schmidt, D. Wegener and J. Bleckwenn, Nucl. Phys. B 32 (1971) 221.
[63] O. Benhar, Nucl. Phys. A 476 (1988) 272.
[64] J.L. Friar, Ann. of Phys. 81 (1973) 332.
[65] J.D. Walecka, Nucl. Phys. A 399 (1983) 387.
[66] T. Matsui, Phys. Lett. B 132 (1983) 260.
[67] G. DoDang, M. L'Huillier, Nguyen Van Giai and J.W. Van Orden, Phys. Rev. C 35 (1987) 1637.
[68] C.R. Chinn, A. Picklesimer and J.W. van Orden, Phys. Rev. C 40 (1989) 790, 1159.
[69] T.W. Donnelly, E.L. Kronenberg and J.W. Van Orden, Nucl. Phys. A 494 (1989) 365.
[70] T.C. Ferrée and D.S. Koltun, Phys. Rev. C 49 (1994) 1961.
[71] Z.E. Meziani, Nucl. Phys. A 446 (1985) 113c.
[72] A. Amroun, V. Breton, J. Cavedon, B. Frois, D. Goutte, F. Juster, P. Leconte, J. Martino, Y. Mizuno, X. Phan, S. Platchkov, I. Sick and S. Williamson, Nucl. Phys. A 579 (1994) 596.
[73] J.M. Cavedon, B. Frois, D. Goutte, M. Huet, Ph. Leconte, C.N. Papanicolas, X.-H. Phan, S.K. Platchkov, S. Williamson, W. Boeglin and I. Sick, Phys. Rev. Lett. 49 (1982) 978.
[74] I. Sick, Phys. Lett. B 116 (1982) 212.
[75] D. Day and I. Sick, Phys. Lett. B 274 (1992) 16.